Research | Open Access

Cholesterol-Rich Plasma Membrane Submicrodomains Can Be a Major Extramitochondrial Source of Reactive Oxygen Species in Partially Depolarized Mature Cerebellar Granule Neurons in Culture

Sofia Fortalezas[1], Joana Poejo[1], Alejandro K Samhan-Arias[2] and Carlos Gutierrez-Merino[1*]

[1]Department of Biochemistry and Molecular Biology, Faculty of Sciences, and Institute of Molecular Pathology Biomarkers, University of Extremadura, 06006- Badajoz, Spain

[2]Department of Biochemistry, Autonomous University of Madrid (UAM), and 'Alberto Sols' Biomedical Research Institute (CSIC-UAM), c / Arturo Duperier 4, 28029-Madrid, Spain

***Corresponding author:** Carlos Gutierrez-Merino, Dept. Biochemistry and Molecular Biology, Faculty of Sciences, and Institute on Molecular Pathology Biomarkers, University of Extremadura, 06006-Badajoz, Tel: 606953213, E-mail: carlosgm@unex.es

Citation: Sofia Fortalezas (2019) Cholesterol-Rich Plasma Membrane Submicrodomains Can Be a Major Extramitochondrial Source of Reactive Oxygen Species in Partially Depolarized Mature Cerebellar Granule Neurons in Culture. J Neurophysiol Neurol Disord 5: 1-22.

Abstract

Excessive production of reactive oxygen and nitrogen species can elicit neuronal cell death and brain neurodegeneration. In previous studies, we have shown that lipid rafts nanodomains of mature cerebellar granule neurons (CGN) contain most of the neuronal nitric oxide synthase and also of cytochrome b_5 reductase isoform 3 (Cb5R3), which is the component of neuronal synaptic plasma membrane vesicles that generates superoxide anion upon stimulation by cytochrome c. In this work, we show that CGN maturation in vitro elicits between two- and three-fold increase of the overall lipid rafts, and a similar increase of the expression of neuronal nitric oxide synthase and Cb5R3. Only 5-15 min incubation of CGN with millimolar concentrations of methyl-β-cyclodextrin led to more than 90% attenuation of the kinetics of reactive oxygen species (ROS) production monitored by dihydro dichlorofluorescein diacetate (H$_2$DCF-DA), dihydroethidium (DHE) and 4,5-diaminofluorescein diacetate (DAF2-DA). In contrast, the results obtained using H$_2$DCF-DA and DHE pointed out that preincubation of CGN with 2,4-dinitrophenol or carbonyl cyanide-4- (trifluoromethoxy) phenylhydrazone (FCCP) only produced a decrease of 38±5% and 42±5% of the rate of ROS production, respectively. In addition, superoxide dismutase added to the extracellular medium of CGN also elicited more than 90% attenuation of the increase of DHE fluorescence that monitors superoxide anion production. CGN maturation leads to a large decrease of the production of ROS detected by H$_2$DCF-DA, and this attenuation of ROS production in mature CGN can be reverted by silencing the expression of Cb5R3 to approximately 50%. The kinetics of ROS/reactive nitrogen species (RNS) production by CGN detected with DAF2-DA revealed the occurrence of a spreading ROS/RNS wave rapidly propagating along the neuronal plasma membrane. In conclusion, our results point out that redox systems associated with lipid rafts make a large contribution to total ROS/RNS production in mature CGN cultures under partially depolarizing conditions.

Keywords: Reactive oxygen and nitrogen species; neuronal lipid rafts; cerebellar granule neurons; methyl-β-cyclodextrin; cytochrome b_5 reductase; neuronal nitric oxide synthase.

Abbreviations

CGN: cerebellar granule neurons; Cb5R: cytochrome $b_5$reductase; Cb5R3: isoform 3 of cytochrome $b_5$reductase; DAF2-DA: 4,5-diaminofluorescein diacetate; DCF: 2',7'-dichlorofluorescein; DHE: dihydroethidium; DIV: days *in vitro*; DMEM: Dulbecco's modified Eagle's medium; DNP: 2,4-dinitrophenol; DPI: diphenyleneiodonium; FCCP: carbonyl cyanide-4- (trifluoromethoxy) phenylhydrazone; FRET: fluorescence resonance energy transfer; Fura2-AM: Fura2 acetoxymethyl ester; GF: green fluorescence; H_2DCF-DA: 2',7'- dihydrodichloro fluorescein diacetate; IC50: half maximal inhibitory concentration; LTCCs: L-type calcium channels; MβCD: methyl-β-cyclodextrin; MnT-BAP: Mn(III)tetrakis (4-benzoic acid) porphyrin chloride; MTT: 3-(4,5-dimethylthiazol-2-yl)-2,5-diphenyltetrazolium bromide; nNOS: neuronal nitric oxide synthase; PVDF: polyvinylidene difluoride; RF: red fluorescence; ROI: region of interest in microscopy images; RNS: reactive nitrogen species; ROS: reactive oxygen species; s.e.: standard error; SIN-1: 3-morpholinosydnonimine; SOD: superoxide dismutase; TBST: Tris-buffered saline (TBS) supplemented with 0.05% polyoxyethylene sorbitan monolaurate; Tiron: 4,5-dihydroxy-1,3-benzene disulfonic acid; Tris: tris–(hydroxymethyl) aminomethane; Triton X-100: 4-(1,1,3,3-tetramethylbutyl) phenyl- polyethylene glycol.

Introduction

Oxidative stress induced by excessive production of reactive oxygen and nitrogen species can elicit neuronal cell death and brain neurodegeneration. This has been shown during last 20 years with neuronal cultures *in vitro* [1-3], with animal models of neurodegenerative diseases [4,5] and brain insults like transient ischemia [6,7], and also in human brains after brain stroke [8] or affected by major neurodegenerative diseases [2,9-12]. At least in part, this is due to the fact that the cerebrospinal fluid is poorer in antioxidants than the blood, because of the low permeability and high selectivity of the blood-cerebrospinal fluid barrier.

Studies with primary cultures of cerebellar granule neurons (CGN) have shown that an overshot of reactive oxygen species (ROS) production plays a critical role for the entry in the irreversible stage of low potassium-induced apoptosis [13-15]. Noteworthy, the peak of this ROS overshot was at approximately 3 h after the change of CGN to low potassium medium, well before the drop of mitochondrial membrane potential and before a significant release of cytochrome *c* from mitochondria to the cytosol [16]. Furthermore, the addition of superoxide dismutase (SOD) to the extracellular medium of CGN cultures quenches more than 90% of this ROS overshot and also blocks the apoptotic process [13,14]. As superoxide anion has a low permeability across lipid bilayers [17], this ROS overshot must have a large component of superoxide anion released to the extracellular medium. Therefore, although mitochondria is widely accepted as the major source of intracellular superoxide anion in oxidative stress-induced neuronal death in cultures in vitro [2,3,18], extramitochondrial ROS production seems to play a major role in the superoxide anion overshot at the onset of CGN apoptosis induced by potassium deprivation of the extracellular medium. On these grounds, the possibility that redox systems of the plasma membrane may be a major sub cellular source of superoxide anion deserves to be studied.

Plasma membrane NADPH oxidases of the NADPH oxidases family play a major role in superoxide anion production in glial, macrophages and endothelial cells [19]. However, we have reported previously that in brain synaptic membranes derived from rat synaptosomes and in CGN cultures the NADPH-dependent superoxide anion production is nearly ten-fold lower than the NADH-dependent superoxide anion production [14,20,21]. In previous works, we have shown that dysregulation of cytochrome b_5 reductase (Cb5R) associated with plasma membrane lipid rafts sub-microdomains is largely responsible for the overshot of superoxide anion observed at the onset of CGN apoptosis induced by 5 mM potassium concentration in the extracellular medium [16,22]. Briefly, our results showed that the mRNA levels of both Cb5R and cytochrome b_5 increases nearly three-fold and an enhanced translocation of Cb5R to the neuronal plasma membrane within 1-3 hours after switching CGN to a 5 mM K^+ medium [16]. The increase of the level of cytochrome b_5 can account for the stimulation of the NADH activity of the plasma membrane of CGN in this time window [14] because cellular cytochrome b_5 concentration is not saturating for Cb5R. It is to be noted that this correlated with the three to four-fold increase of superoxide anion production measured three hours after the change of CGN to a pro-apoptotic low potassium medium [16].

We have shown that the isoform 3 of cytochrome b_5 reductase (Cb5R3) and cytochrome b_5 are highly expressed in the cerebellar granule neurons of the adult rat brain, and also in cerebellar Purkinje cells and pyramidal neurons of the brain neocortex and neuronal motor nuclei of the brain stem [23]. Therefore, dysregulation of Cb5R3 is also likely to play a widespread role in brain neuronal degeneration in oxidative stress-mediated apoptosis and not only in CGN apoptosis. It is to be recalled here that over 40 mutations of Cb5R3 have been linked to recessive congenital type II methemoglobinemia [24,25]. In persons affected by this rare disease mild cyanosis is accompanied by generalized

dystonia, movement disorders, failure to thrive, and cortical and subcortical atrophy [24-27], including cerebellar atrophy [28].

Neuronal nitric oxide synthase (nNOS) is another redox system that is tightly associated with plasma membrane lipid rafts in neurons [29-31], and in previous works, we have shown that nNOS and Cb5R3 co-localize within caveolin-1-rich lipid rafts of mature CGN in culture [30,31]. Nitric oxide overproduction has been widely noticed in oxidative stress-induced brain degeneration [8]. Nitric oxide reaction with superoxide anion yields peroxynitrite [32], one of the most neurotoxic ROS generated during oxidative stress-induced brain neurodegeneration as excitotoxic neuronal death elicited by L-glutamate through activation of N-methyl D-aspartate receptors [2,33], brain ischemia-reperfusion [8], inflammation and spinal cord injury [34,35], neurodegenerative diseases and aging [2,9].

Methyl-β-cyclodextrin (MβCD) has been extensively used for cholesterol removal and lipid rafts disruption in different cell lines [36,37], and also in mature CGN in culture in a recent study of our laboratory [38]. Noteworthy, cyclodextrins are also used as antibrowning additives in foods and foodstuffs [39], as well as additives to improve the bioavailability of poorly soluble drugs [40,41].

The main goal of this work has been to evaluate in partially depolarized CGN cultures the contribution of ROS production and in particular of superoxide anion by redox systems associated with lipid rafts of the plasma membrane relative to mitochondrial production of these ROS. This study has been performed with mature CGN and also during maturation of CGN in culture, to seek for correlations between the increase of protein markers of lipid rafts, Cb5R and nNOS expression during CGN maturation and the overall ROS production and sensitivity to exposure to extracellular peroxynitrite. The results show that the redox systems associated with lipid rafts of the CGN plasma membrane can account for a production of ROS in partially depolarized CGN in culture much higher than usually recognized.

Materials and Methods

Preparation of rat cerebellar granule neurons (CGN)

CGN have been prepared from Wistar rats as described previously [14,22,30,31,38,42-44]. Animal handlings were performed in accordance with Spanish regulations and were approved by the Ethical Committee of the University of Extremadura. CGN cultures were kept at 37 °C in a humidified atmosphere of 95% air/5% CO$_2$. Cytosine arabinofuranoside (10 µM) was added to fresh culture medium 48 h after plating to pre-

vent replication of non-neuronal cells. Seven days after plating, the culture medium was replaced with the following serum-free Dulbecco's modified Eagle's medium (DMEM):F12 medium (1:1) supplemented with 12.5 mM glucose, 20.82 mM KCl, 5 µg/mL insulin, 0.1 mg/mL apo-transferrin, 20 nM progesterone, 50 U/mL penicillin, 25 U/mL streptomycin, 1.1 mM pyruvate and 2 mM L-glutamine. The extracellular medium was changed 30 minutes before running fluorescence microscopy and cell viability experiments to MLocke's K25 buffer (pH 7.4 at 37 ºC): 4 mM NaHCO$_3$, 10 mM Tricine, 5 mM glucose, 2.3 mM CaCl$_2$, 1 mM MgCl$_2$ and 134 mM NaCl/25 mM KCl. Cell viability was experimentally assessed measuring the amount of colored formazan by the reduction of 3-(4,5-dimethylthiazol-2-yl)-2,5-diphenyltetrazolium bromide (MTT) as in previous works [14,31,42-44].

Fluorescence microscopy

CGN in Petri plates were kept at 37ºC in MLocke's K25 in the thermostated plate holder of the epifluorescence microscope for image acquisition. Fluorescence microscopy images of CGN have been acquired with a Hamamatsu Orca-R^2 CCD camera (binning mode 2 x 2) attached to a Nikon Diaphot 300 epifluorescence microscope (Tokyo, Japan) with an NCF Plan ELWD 40× objective. Quantitative analysis of the average fluorescence intensity per pixel of selected neuronal soma was done with the HCImage software using the region of interest (ROI) tool of this software, as in previous works [31,38,44]. Only fields devoid of large aggregates of neurons forming granules or small grain-like structures were selected for image acquisition, to minimize distortion of images by the sum of the fluorescence contributions of juxtaposed layers of neurons. The mean ± s.e. intensity reading of fluorescence per pixel within CGN somas were obtained in experiments performed by triplicate (n>100 CGN somas in each case). 2',7'-dihydrodichloro fluorescein diacetate (H$_2$D-CF-DA), a broad-range ROS indicator [45], has been used as an indicator of the overall oxidative stress. Dihydroethidium (DHE) has been used as an indicator of superoxide anion production [46,47]. 4,5-diaminofluorescein diacetate (DAF2-DA) has been used to monitor nitric oxide and ROS production upon the rapid reaction of nitric oxide with superoxide anion and ascorbate free radicals [48]. For image acquisition in this work, these dyes were added at the following concentrations: 10 µM (H$_2$DCF-DA and DHE) and 5 µM (DAF2-DA). Images of CGN stained with H$_2$DCF-DA, cholera toxin B-Alexa 488 and DAF2-DA have been acquired with an excitation filter of 470 nm, and 510 nm dichroic mirror/520 nm emission filter (green fluorescence), using an exposure time of 0.5 s for H$_2$DCF-DA, 0.1 s for cholera toxin B-Alexa 488 and 0.05 s for DAF2-DA. Images of CGN stained

with DHE have been acquired with an excitation filter of 470 nm, and 580 nm dichroic mirror/590 nm emission filter (red fluorescence), using an exposure time of 0.05 s.

The mitochondrial contribution to the production of ROS by CGN in MLocke's K25 has been evaluated using the uncoupling agent carbonyl cyanide-4- (trifluoromethoxy) phenylhydrazone (FCCP) and 2,4-dinitrophenol (DNP) added to the extracellular medium 10 minutes before the addition of H_2DCF-DA or DHE.
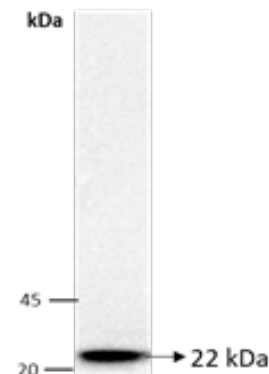
Cell lysates and Western blotting

CGN have been lysed in buffer 25 mM tris-(hydroxymethyl) aminomethane (Tris)–HCl, pH 7.4, 150 mM NaCl, 5 mM ethylenediaminetetraacetic acid, 50 mM NaF, 5 mM $NaVO_3$ and 0.25 % 4-(1,1,3,3-tetramethyl butyl)phenyl- poly-ethylene glycol (Triton X-100), supplemented with 1x SIGMA-FAST^{TM} protease inhibitor cocktail (Sigma-Aldrich). Lysates were collected and supplemented with 50% glycerol and stored at -80ºC until use. The protein concentration of cell lysates was measured with Bradford's method, using bovine serum albumin as standard.

CGN lysates (20 µg of protein per lane) were loaded in 7.5-12.5% acrylamide SDS- PAGE gels. Once the electrophoresis run was finished, the gel was transferred to polyvinylidene difluoride (PVDF) membranes of 0.2 µm average pore size (Trans-BloT Transfer Medium, Bio-Rad). Afterward, PVDF membranes were blocked with 3% bovine serum albumin in Tris-buffered saline (TBS) supplemented with 0.05% polyoxyethylene sorbitan monolaurate (TBST). Before the incubation with the primary antibody, membranes were washed three times with TBST. The immunodetection of the selected proteins was performed with their specific primary antibody at a dilution of 1:200 in TBST. Primary antibodies used for Western blotting: goat anti-H-Ras (Santa Cruz Biotechnology, sc-32026), rabbit anti-caveolin-1 (Santa Cruz Biotechnology, sc-894), mouse anti-nNOS (Santa Cruz Biotechnology, sc-5302), and rabbit anti-Cb5R3 (ProteinTech 10894-1-AP). These primary antibodies give a major stained band at the expected protein molecular weight of the target protein in Western blotting run with CGN lysates (*Supplementary Figure S1*). After incubation with the first antibody overnight, membranes were washed six times with TBST and incubated for 1 h at room temperature with the appropriate secondary IgG antibody conjugated with horseradish peroxidase. Secondary antibodies, anti-rabbit IgG-Horseradish peroxidase, anti-goat IgG-Horseradish peroxidase, and anti-mouse IgG-Horseradish peroxidase, were used at a dilution of 1:25,000,

1:10,000 and 1:5,000 in TBST, respectively. Again, we washed the membrane six times with TBST followed by incubation for 3 min with Bio-Rad Clarity Western ECL substrate. Western blots were revealed with Bio-Rad ChemiDoc TM XRS+. Then, membranes were treated under continuous stirring at room temperature with the following stripping buffers: (1) 10 min with 0.2 M glycine/0.5 M NaCl brought to pH 2.8 with acetic acid and (2) 10 min with M acetic acid/0.5 M NaCl at pH 2.5. After washing with distilled water during 10 min, membranes were blocked with 3% bovine serum albumin in TBST and treated as indicated above to quantify β-actin to monitor protein load, using mouse anti-β-actin (Sigma-Aldrich-A1978, 1:200 dilution) or rabbit anti-β-actin (Sigma-Aldrich- A5060, 1:200 dilution) as primary antibody and anti-mouse IgG-Horseradish peroxidase (1:5,000 dilution) or anti-rabbit IgG-Horseradish peroxidase (1:25,000 dilution) as secondary antibody.
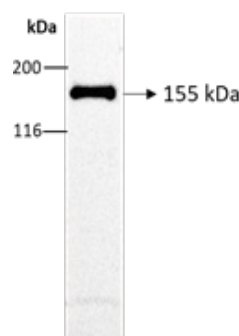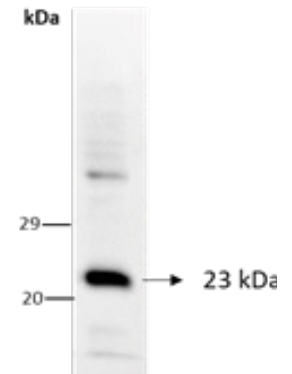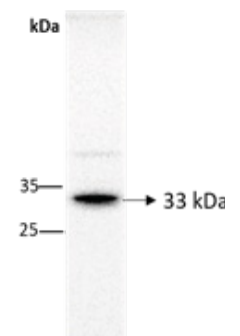

Supplementary Figure S1. Western blotting of CGN lysates with the primary antibodies used in this work.

The detection and specificity of primary antibodies for their corresponding target proteins in CGN lysates was confirmed by Western blotting: rabbit anti-caveolin-1 (sc-894), goat anti-H-Ras (sc-32026), mouse anti- nNOS (sc-5302) and rabbit anti-Cb5R3 (ProteinTech-10894-1-AP). SDS-PAGE were loaded with 20 μg of protein of CGN lysates per lane. All primary antibodies have been used at a dilution of 1:100 in TBST. Secondary antibodies, anti-rabbit IgG-Horseradish peroxidase, anti-goat IgG-Horseradish peroxidase and anti-mouse IgG- Horseradish peroxidase, were used at a dilution of 1:25,000, 1:10,000 and 1:5,000 in TBST, respectively. See Materials and Methods for further experimental details.

Fluorescence measurements of cholera toxin B-Alexa 488 bound to resuspended CGN.

Measurements of cholera toxin B-Alexa 488 bound to CGN have been performed by fluorimetry as in [22]. Briefly, after washing the Petri plates with 1mL of MLocke's K25 buffer and careful resuspension of the cells in 2 mL of MLocke's K25 buffer +1% polyoxyethylene sorbitan monolaurate, cholera toxin B-Alexa 488 bound to resuspended CGN was measured with a fluorimeter Perkin-Elmer 650-40 in a thermostated cuvette under mild stirring at 37ºC, with excitation and emission wavelengths of 470 and 520 nm and slits-width of 10 nm.

Fluorescence Resonance Energy Transfer (FRET) imaging

FRET imaging has been performed as in previous works [16,30,31,49], with CGN at the indicated days *in vitro* (DIV) in 24-well plates with 600,000 cells per well or in 35 mm diameter Petri plates with 2.5×10^6 cells per plate. The plates were washed twice with 1 mL MLocke's K25 buffer to wash the phenol red remaining in the plates. Then CGN were fixed with 2.5% paraformaldehyde, 3 mM $MgCl_2$, 2 mM ethylene glycol- bis (2-aminoethyl ether)-N,N,N′,N′-tetraacetic acid and 0.32 M sucrose in PBS's buffer (5 mM sodium phosphate, 137 mM NaCl and 27 mM KCl, pH 7).

The selected protein targets for FRET imaging have been: H-Ras, caveolin-1 and neuronal nitric oxide synthase (nNOS). Before their use for fluorescence microscopy images acquisition, the specificity of primary antibodies for the selected target proteins was routinely assessed by the presence of a major band at the expected protein molecular weight accounting for more than 90% bands staining in Western blotting run with CGN lysates. Primary antibodies used in these experiments: goat anti-H-Ras (Santa Cruz Biotechnology, sc-32026), rabbit anti-caveolin-1 (Santa Cruz Biotechnology, sc-894) and mouse anti-nNOS (Santa Cruz Biotechnology, sc-5302). (*Supplementary Figure S1*).

After fixation, different CGN plates were incubated during 1 h at 37 °C with the first antibody against the target protein-1 or against the target protein-2 (1:100 dilution) in PBS supplemented with 0.2% Triton X-100, and then washed six times with PBS (washing step). Thereafter, CGN plates incubated with the antibody against the target protein-1 were incubated for 30 min with the appropriate Alexa488-labelled secondary antibody (1:200 dilution) in PBS supplemented with 0.2% Triton X-100 and washed again with PBS before the acquisition of fluorescence microscopy images stained only with the donor dye. These CGN plates will be named as (target protein- 1)**A488. CGN plates incubated with the antibody against the target protein-2 were incubated for 30 min with the appropriate Cy3-labelled secondary antibody (1:200 dilution) in PBS supplemented with 0.2% Triton X-100, and washed again with PBS before acquisition of fluorescence microscopy images stained only with the acceptor dye. These CGN plates will be named as (target protein-2)**Cy3. After finishing the acquisition of the images of these plates, CGN plates (target protein-1) **A488 were incubated during 1 h at 37 °C with the second primary antibody against target protein-2 in PBS supplemented with 0.2% Triton X-100, washed six times with PBS (washing step), and then incubated for 30 min with the appropriate Cy3-labelled secondary antibody in PBS supplemented with 0.2% Triton X-100, and finally washed again with PBS. These CGN plates will be named as (target protein-1)**A488/ (target protein-2)**Cy3. The lack of significant fluorescence labelling of CGN treated with the Alexa488- and Cy3-secondary IgG antibodies used in this study in the absence of the primary antibodies was assessed before running FRET experiments, confirming that it yielded fluorescence intensity readings within the background range of control non- stained CGN. Control experiments were performed to quantify the effect of the treatment for labeling with the second primary antibody/IgG-Cy3 complex in the ratio between red and green fluorescence intensities (Ratio RF/GF) of CGN plates (target protein-1)**A488. To this end, CGN were subjected to treatments mimicking those followed for labeling with the second primary antibody (see above) but without the second primary antibody. These control experiments showed that on average the treatment done to label CGN plates (target protein-1)**A488 with the red fluorescent IgG-Cy3 secondary antibody resulted in a small increase of the Ratio RF/GF of 0.15±0.05 units, due to a 20-25% loss of Alexa488 fluorescence intensity. All the results of the Ratio RF/GF obtained with CGN plates (target protein-1)**A488 have been corrected for this effect. Image acquisitions of CGN double-stained with

donor and acceptor dyes, plates (target protein-1)**A488/(target protein-2)**Cy3, were routinely started between 2 and 3 hours after finishing the acquisition of images of CGN stained only with the donor dye, plates (target protein-1)**A488. Finally, the exposure times were fixed at 0.3 s, i.e. as low as possible to ensure that the contribution of CGN autofluorescence was always lower than 10% of the fluorescence intensity readings of cells stained with the primary and secondary antibodies used in this work.

The average intensity of fluorescence per pixel within CGN somas were taken using the ROI tool of the Hamamatsu HC Image software to select somas as areas of interest in experiments performed by triplicate (n>200 CGN somas in each case). Images of CGN stained only with anti-H-Ras/IgG-Cy3 (H-Ras*-Cy3) were acquired to substract the direct excitation component of the red fluorescence intensity per pixel. As discussed in previous works [30,31,49], significant FRET efficiency using this experimental approach implies that the selected protein pair is separated by ≤80 nm.

Measurement of the intracellular free Ca^{2+} concentration ($[Ca^{2+}]_i$)

$[Ca^{2+}]i$ was measured as in previous works of our laboratory [31,38,42-44]. Briefly, CGN were loaded with Fura2 by incubation in DMEM-F12 for 60 min with 5 μM Fura-2-acetoxymethyl ester (Fura2-AM) and 0.025% Pluronic-F127 at 37°C. Then CGN was washed and the culture dish placed in the thermostatic controlled plate (Warner Instrument Co., Hamden, CT) of the Nikon Diaphot 300 inverted epifluorescence microscope. Digital images with 340 and 380 nm excitation filters and 510 nm dichroic mirror/520 nm emission filter were taken with a Hamamatsu Orca-R^2 CCD camera (binning mode 2 x 2) and Lamdba 10–2 filter wheel controller and subsequently analyzed with HCImage software. Data acquisition and analysis were done after the selection of the neuronal soma using the region of interest (ROI) tool of this software. Ratio 340/380 data given in this work are population averages±s.e. intensity reading of fluorescence per pixel within CGN somas were obtained using the ROI tool of the Hamamatsu HCImage software to select somas as areas of interest in experiments performed by triplicate (n>100 CGN somas in each case).

Cb5R3 silencing in CGN

For siRNA knockdown studies Accell™ siRNA delivery system was used (Dharmacon^TM). To knockdown $Cb5R3$ we used the E-089102-00-0005 Accell Rat Cyb5r3 (25035) siRNA SMART pool and as control was used the D-001910-10-05 Accell Non-targeting pool. siRNAs were prepared following the instructions of the manufacturer. Briefly, 5x siRNA Buffer was diluted to 1x siRNA Buffer using sterile RNase-free water; a 100 μM siRNA solution was prepared in 1x siRNA buffer and up and down 3-5 times while avoiding introduction of bubbles; the solution was placed on an orbital mixer/shaker for 90 minutes at 37 °C and briefly centrifuged to collect solution from the bottom of the tube. In separate tubes the 100 μM siRNA was mixed with Accell Delivery Media 1:100 (delivery mix). CGN were prepared as previously described and at DIV 4 the growth medium was replaced by 500 μL of the appropriate delivery mix to each well (12 wells plate). Cells were incubated at 37 °C with 5% CO2 for 90 hours for Western blotting analysis, or by 72 hours for fluorescence microscopy measurements. Thereafter, cell lysates for Western Blotting or fluorescence microscopy measurements of ROS production with H_2DCF-DA were performed as described above.

Chemicals and reagents

H_2DCF-DA was purchased from Molecular Probes (Life Sciences Technologies, Carlsbad, CA, USA). DHE and DAF2-DA were obtained from the Spain office of Sigma (St. Louis, MO, USA). Cholera toxin B-Alexa 488 (cat. number C22841) and Mn (III) tetrakis (4-benzoic acid) porphyrin chloride (MnTBAP) were obtained from Invitrogen (Molecular Probes, Eugene, OR, USA).Fura2-AM from Invitrogen (Life Sciences Technologies) was supplied by Thermo Fisher Scientific (Spain office). Primary antibodies: goat anti-H-Ras (sc-32026), rabbitanti-caveolin-1 (sc-894), mouse anti-nNOS (sc-5302) and goat anti-CYP46 (sc-74391) were supplied by Santa Cruz Biotechnology (Santa Cruz, CA, USA); rabbit anti-$Cb5R3$ (ProteinTech 10894-1-AP); mouse anti-β-actin (A1978) and rabbit anti-β- actin (A5060) were supplied by Sigma-Aldrich (Spain office). Fluorescent secondary antibodies: anti-rabbit IgG-Alexa488 (cat.number A11008) and anti-mouse IgG- Alexa488 (cat. number A11001) from Invitrogen (Molecular Probes, Eugene, OR, USA), and anti-goat IgG-Cy3 (cat. number C2821) from the Spain office of Sigma (St. Louis, MO, USA). All these antibodies were used in the dilution range recommended in their technical sheets. Anti-rabbit IgG-Horseradish peroxidase and anti-mouse IgG- Horseradish peroxidase were supplied by Sigma-Aldrich. Anti-goat IgG-Horseradish

peroxidase was supplied by Pierce (Rockford, IL, USA). Bio-Rad Clarity Western ECL substrate was purchased to Bio-Rad (Spain office). Accell™ siRNA delivery system was supplied from Dharmacon (Lafayette, Colorado, USA), with the E- 089102-00-0005 Accell Rat Cyb5r3 (25035) siRNA SMART pool to knockdown C*b*5R3, and the D-001910-10-05 Accell Non-targeting pool as control. Tetrodotoxin was obtained from Sankyo Co. (Tokyo, Japan).

All other reagents and chemicals used were of analytical grade from Sigma-Aldrich (Spain office) or Roche-Merck (Darmstadt, Germany).

Statistical analysis

Results are expressed as mean ± standard error (s.e.). Statistical analysis was carried out by Mann–Whitney non-parametric test. A significant difference was accepted at the $p < 0.05$ level. All the results were confirmed with at least triplicate measurements with different CGN preparations.

Results

Treatment of CGN with millimolar concentrations of methyl-β-cyclodextrin for 5-15 min led to more than 90% attenuation of the kinetics of ROS production monitored by the ROS-sensitive fluorescent dyes H$_2$DCF-DA and DHE.

Selected representative images of fluorescence microscopy of mature CGN in MLocke's K25 stained with H$_2$DCF-DA and DHE are shown in Figure 1. The intensity of fluorescence of these dyes is clearly higher in the neuronal somas. In addition, the long dendritic extensions connecting distant neuronal somas are more intensely stained with H$_2$DCF-DA than with DHE. Indeed, these extensions are hardly seen with the red fluorescence of DHE staining. We have acquired images of DHE staining after preincubation for 1.5 hours with the superoxide anion scavenger 4,5-dihydroxy-1,3-benzene disulfonic acid (Tiron)[50,51], to evaluate the putative contribution to the measured DHE fluorescence of DNA- and RNA-oxidized ethidium complexes formation [45,46]. The results shown in Figure 1C revealed that the intensity of red fluorescence of DHE in the neuronal somas of CGN was largely quenched, approximately 70 % quenching, by 20 mM Tiron, pointing out that it was largely due to the formation of superoxide anion-mediated oxidation of DHE. Therefore, the analysis of these images led to the conclusion that the neuronal somas produced most of the superoxide anion generated by mature CGN in culture, and that its production along the large dendritic extensions it is rather low compared with the production of other ROS.
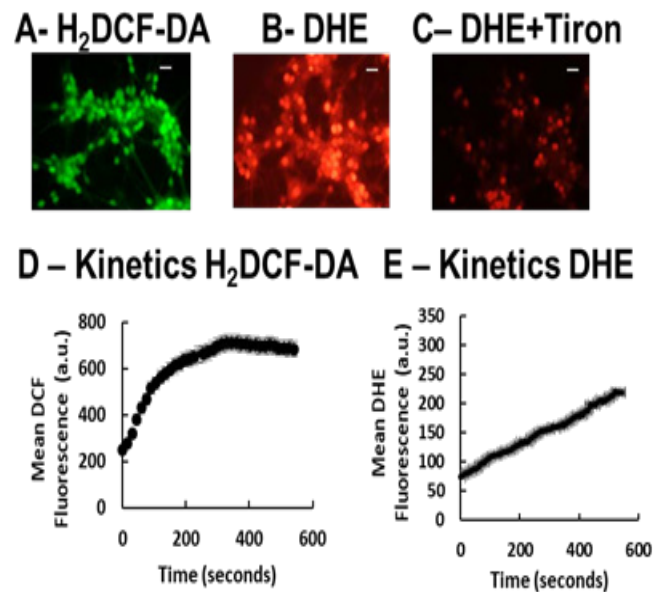
Figure 1. H$_2$DCF-DA and DHE monitors ROS production upon incorporation to CGN. Representative fluorescence microscopy images of mature CGN showed that they accumulated a significant amount of DCF (**Panel A**) and oxidized DHE (**PanelB**) only after 10 min of addition of 10 μM H$_2$DCF-DA and DHE to MLocke's K25. Addition of 20 mM Tiron to the extracellular medium 1 hour before the addition of DHE largely attenuated the increase of DHE fluorescence (**Panel C**). The kinetics of an increase of the average fluorescence intensity per pixel in the soma of mature CGN after the addition of H$_2$DCF-DA and DHE to MLocke's K25 medium is shown in **Panels D** and **E**, respectively. Scale bar inserted in fluorescence microscopy images = 10 μm.

The kinetics of increase of fluorescence intensity upon addition of these dyes to the extracellular medium of mature CGN in culture is shown in Figure 1D-E. The kinetics of the increase of fluorescence observed upon addition of H$_2$DCF-DA to the extracellular medium of CGN is complex, with three defined phases: (1) an initial short delay phase, (2) an almost linear rise phase, and (3) a delayed fluorescence decrease phase, likely due to release of the de-esterified dye to the extracellular medium. Due to this, as an index of the relative rate of ROS production by CGN using H$_2$DCF-DA we have taken the maximum slope of the second phase of the increase of fluorescence or the increase of fluorescence intensity after 5 minutes. In contrast, the kinetics of the increase of fluorescence observed with DHE showed a sustained linear increase of fluorescence in the minute's scale range, and we have used the slope of this linear increase as an index of the relative rate of superoxide anion production by CGN.

The treatment of CGN during 20 min with millimolar methyl-β-cyclodextrin (MβCD) concentrations was highly effective in cholesterol removal from these neurons, as 5 mM MβCD elicited approximately 80% of the maximum depletion of cholesterol, confirming our previous observation [38]. MTT

measurements showed that this treatment with MβCD did not produce a significant decrease of cell viability, i.e. 95±5% cell viability with respect to controls of untreated CGN.

As the shorter the incubation time with MβCD, the cholesterol removal should be more restricted to the CGN plasma membrane, in this work we have fixed 5 min the incubation time for MβCD titrations. The incubation of CGN during 5 min with MβCD produced a dose-dependent reduction of the increase of fluorescence after the addition of the fluorescent dyes H_2DCF-DA and DHE, with a half-maximal inhibitory concentration (IC50) of submillimolar MβCD (**Figure 2**). This was not due to quenching of the fluorescence of these dyes by millimolar concentrations of MβCD, as titration of their fluorescence with MβCD in buffer MLocke's K25 produced less than 10% quenching. Noteworthy, the IC50 value of MβCD obtained for H_2D-CF-DA was nearly 10-fold lower than the IC50 value obtained for DHE. The results showed that 5-15 min incubation of CGN with millimolar concentrations of MβCD before the addition of H_2DCF-DA and DHE led to more than 90% attenuation of the increase of fluorescence of these dyes. In addition, as shown with H_2DCF-DA the extent of attenuation of the increase of fluorescence was clearly lowered when CGN were preincubated with cholesterol-MβCD complexes instead of only MβCD (Figure2C).
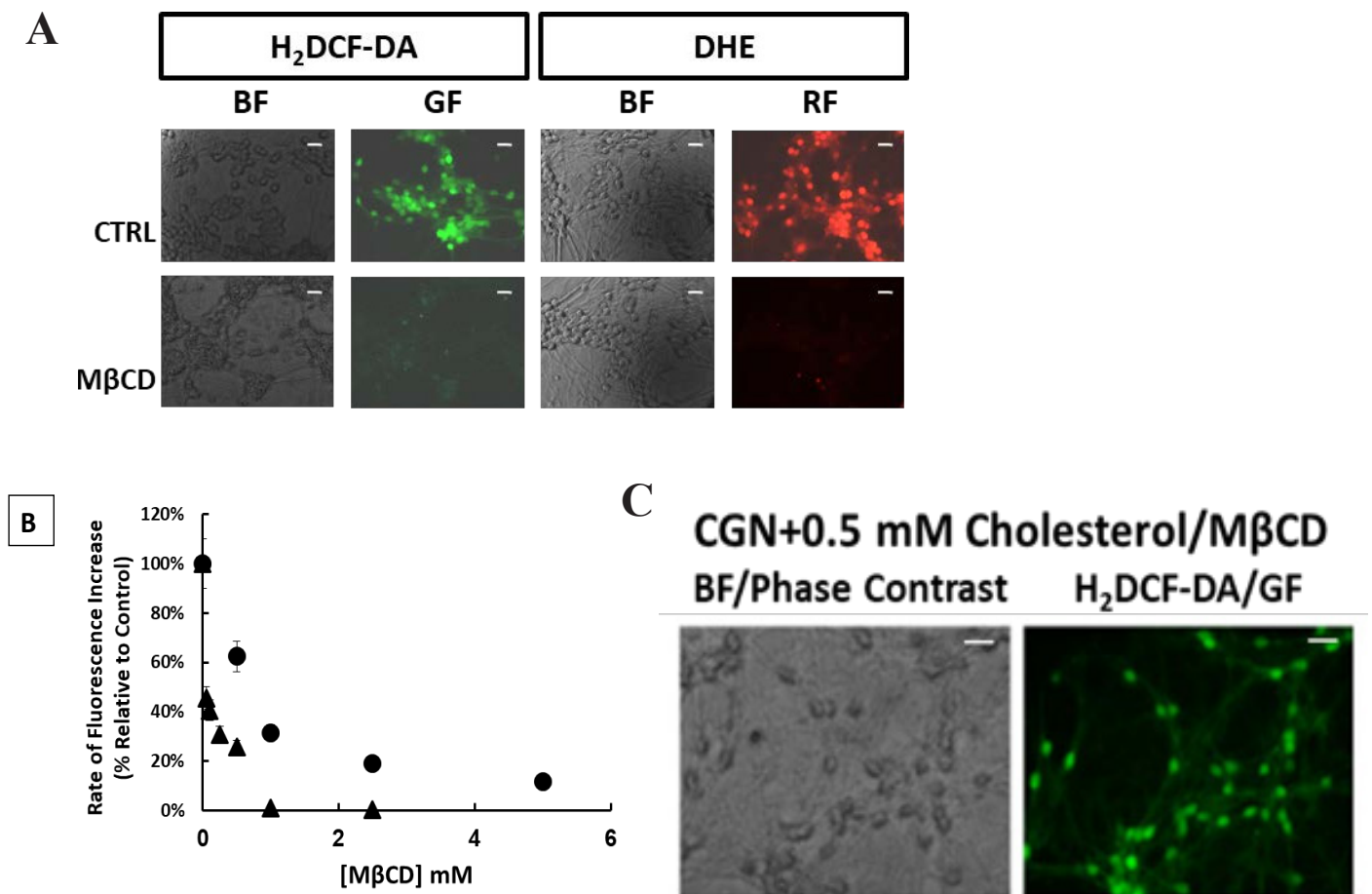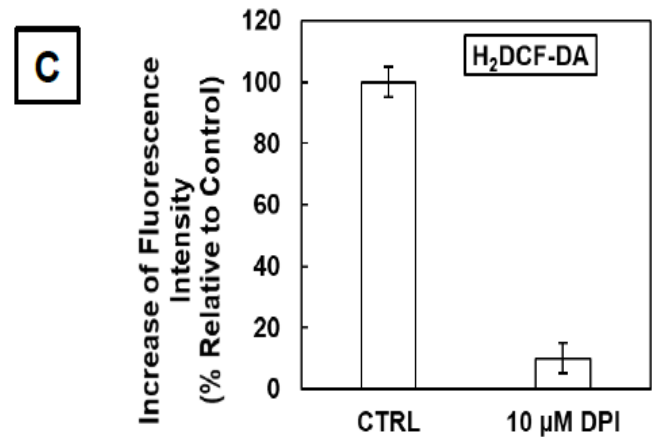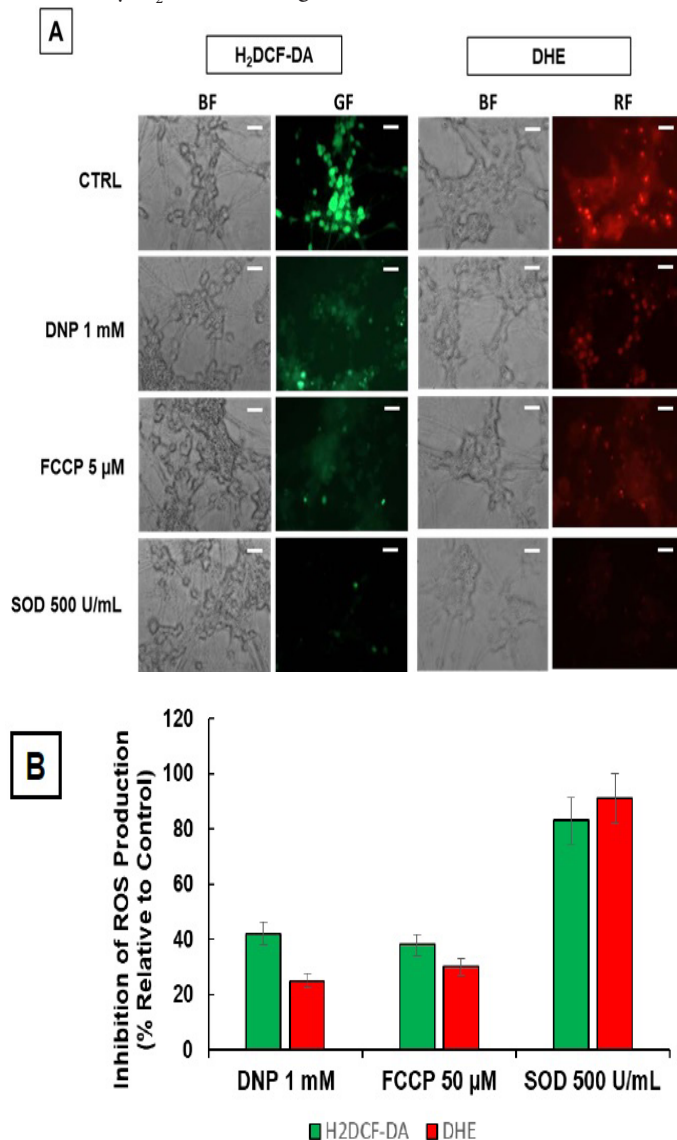

Figure 2. The production of ROS detected by H_2DCF-DA and DHE in mature CGN is more than 90% inhibited by MβCD. Panel A: Representative fluorescence microscopy images show that treatment of CGN with 0.5-1 mM MβCD during 5 min almost completely blocks the increase of fluorescence associated with the production of ROS detected by H_2DCF-DA or DHE addition to the medium. Bright-field (BF), green fluorescence (GF) and red fluorescence (RF) images are shown for each one of the selected fields. **Panel B:** Dependence of the rate of ROS production upon MβCD concentration by 5 min treatment of CGN with MβCD. The rate of ROS production (means± s.e.) has been determined from the maximum slope of the kinetics of an increase of the average fluorescence intensity per pixel in CGN somas of DCF (solid triangles) or of oxidized DHE (solid circles). **Panel C:** The increase of fluorescence intensity per pixel in CGN somas of DCF after 5 min, mean ± s.e., was approximately 60% of the increase recorded for controls when CGN were preincubated with 0.5 mM cholesterol-MβCD complexes instead of only MβCD. Phase-contrast or bright field (BF) and green fluorescence (GF) images are shown for a representative selected field. Scale bar inserted in fluorescence microscopy images = 10 μm.

Mitochondrial and extramitochondrial contribution to ROS production of mature CGN in MLocke'sK25.

The effects on ROS production by CGN in MLocke's K25 of the mitochondrial uncouplers FCCP and 2,4-dinitrophenol (DNP) added to the extracellular medium 10 minutes before the addition of H_2DCF-DA or DHE are shown in Figure 3. These results led to the conclusion that 2,4-dinitrophenol or FCCP only produced a decrease of 38±5% and 42±5% of the rate of ROS production monitored by H_2DCF-DA and DHE, respectively.

In contrast, the addition of SOD to the medium, a cell impermeable superoxide anion scavenger, produced more than 90% decrease of the production of ROS monitored by H_2D-CF-DA or DHE (Figure 3). Furthermore, addition to the extracellular medium of micromolar concentrations of the generic flavoprotein inhibitor diphenyleneiodonium (DPI) also elicited a rapid and complete blockade of the ROS production by CGN detected by H_2DCF-DA (Figure 3C).

Figure 3. The production of ROS detected by H_2DCF-DA and DHE in mature CGN is almost completely inhibited by SOD and DPI, but it is only partially inhibited by DNP or FCCP. Panel A:10 min preincubation with 1 mM DNP or 5 µM FCCP inhibits ≤40% of ROS production detected by H_2DCF-DA or DHE in CGN between 8 and 10 DIV, while it is almost completely inhibited by addition of 500 U/mL SOD only 5 min before of H_2DCF-DA or DHE addition. Bright-field (BF), green fluorescence (GF) and red fluorescence (RF) images are shown for each one of the selected fields. Scale bar inserted in fluorescence microscopy images =10µm. **Panel B:** Percentage of inhibition of ROS production by 1 mM DNP, 5 µM FCCP and 500 U/mL SOD relative to controls, calculated from the increase of the average±s.e. fluorescence intensity per pixel in CGN somas 5 min after addition of H_2DCF-DA or DHE to MLocke's K25 medium. **Panel C:** The inhibition of ROS production after 5 min preincubation with 10 µM DPI relative to controls is also shown by the large attenuation produced by DPI on the increase of the average fluorescence intensity per pixel in CGN somas 5 min after addition of H_2DCF-DA to MLocke's K25 medium.

CGN maturation in vitro leads to an approximately 2 to 3-fold increase of the overall lipid rafts network of these neurons from 4 to 9 days in vitro, and a similar increase of the expression of nNOS.

CGN maturation has been experimentally assessed measuring the contribution of L-type calcium channels (LTCCs) activity to the cytosolic calcium homeostasis because of LTCCs activity increases during CGN maturation in the partially depolarized medium [52]. The decrease of the fluorescence ratio 340/380 of Fura2-loaded CGN in MLocke's K25 medium by the LTCCs inhibitor nifedipine is negligible at 4 DIV and increased from 6 DIV, reaching a maximum decrease value of 0.5 at 8-9 DIV, i.e. from 1.05±0.05 to 0.55±0.05 in the absence and presence of 10 µM nifedipine, respectively (Figure 4A). Staining with fluorescent cholera toxin B-Alexa 488 demonstrated that lipid rafts are widely present in the plasma membrane of CGN in culture (Figure 4B). Moreover, quantitative fluorescence images acquired with the same exposure time and camera gain showed that they increase about two-fold during the *in vitro* CGN mat-

uration process (Figure 4B). This point was also confirmed with fluorescence intensity measurements of cell lysates using a fluorimeter (Figure 4C). The increase is widespread within the neurons, but it is more readily seen at neuronal somas and interdendritic contact sites (Figure 4B).
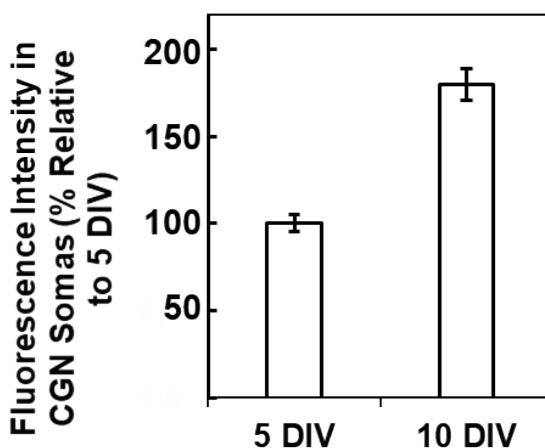
A

B
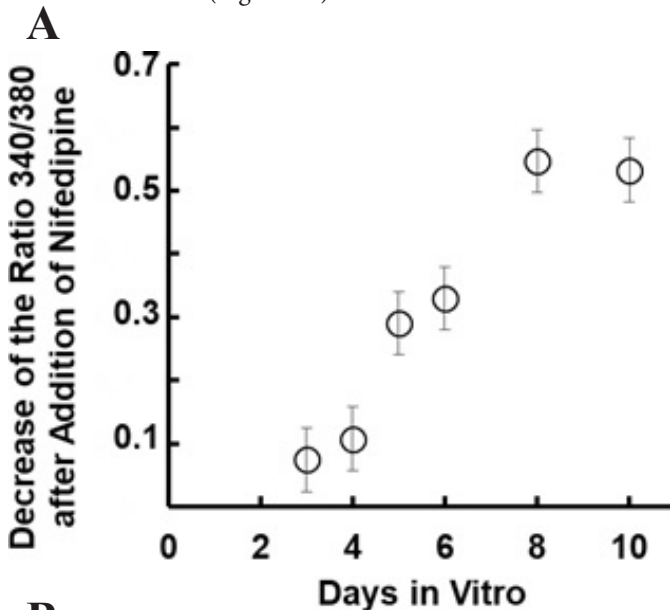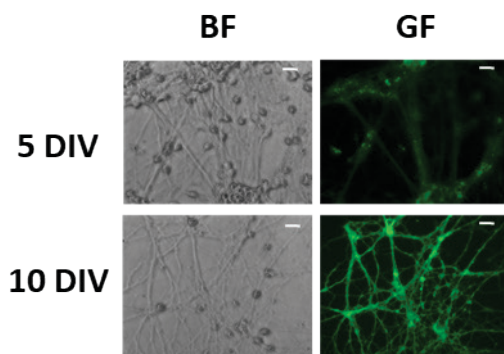
C

Figure 4. Staining of CGN with cholera toxin B-Alexa 488 monitors lipid rafts increase during CGN maturation *in vitro*. Panel A: Dependence upon DIV of the decrease of the ratio (340/380) of the fluorescence of Fura2-loaded CGN after the addition of 10 μM of the LTCCs blocker nifedipine. See Materials and Methods for experimental details of CGN loading with Fura2-AM, image acquisition and ratio (340/360) calculations. **Panel B:** Representative fluorescence microscopy images of non-mature (5 DIV) and mature CGN (10 DIV) stained by 1-hour incubation at 37ºC and 5% CO2 with 1 μg cholera toxin B-Alexa 488, and washed with 1 mL MLocke's K25 medium immediately before images acquisition. Brightfield (BF) and green fluorescence (GF) images are shown for each one of the selected fields. Scale bar inserted in fluorescence microscopy images = 10 μm. **Panel C:** Quantitative fluorimetric analysis of cholera toxin B-Alexa 488 bound to CGN resuspended as indicated in the Materials and Methods. The results yielded a nearly two-fold increase, 1.8±0.2 (mean of triplicate experiment ± s.e.), of the fluorescence of CGN-bound cholera toxin B-Alexa 488 from 5 to 10DIV.

To further assess the increase of lipid rafts during CGN maturation *in vitro* we have measured the expression level of H-Ras and caveolin-1, which are protein-lipid rafts markers in mature CGN [30,31,49]. Western blotting results showed that CGN maturation *in vitro* leads to ≥2- fold increase of H-Ras and~4-fold increase of caveolin-1 from 4 to 9 days *in vitro* (Figure 5). The expression level of nNOS, a protein also associated with CGN lipid rafts, increases approximately 2.5-fold during CGN maturation (Figure 5).

Furthermore, in this work, we show by fluorescence microscopy imaging using anti-caveolin-1 stained with IgG-Alexa 488 and anti-H-Ras stained with IgG-Cy3that caveolin-1 and H-Ras are within FRET distance in fixed mature CGN (Figure 6). In this work, we have experimentally confirmed by FRET microscopy imaging that nNOS is also within FRET distance from H-Ras (Figure 7), i.e. both proteins co-localize within the same lipid rafts.
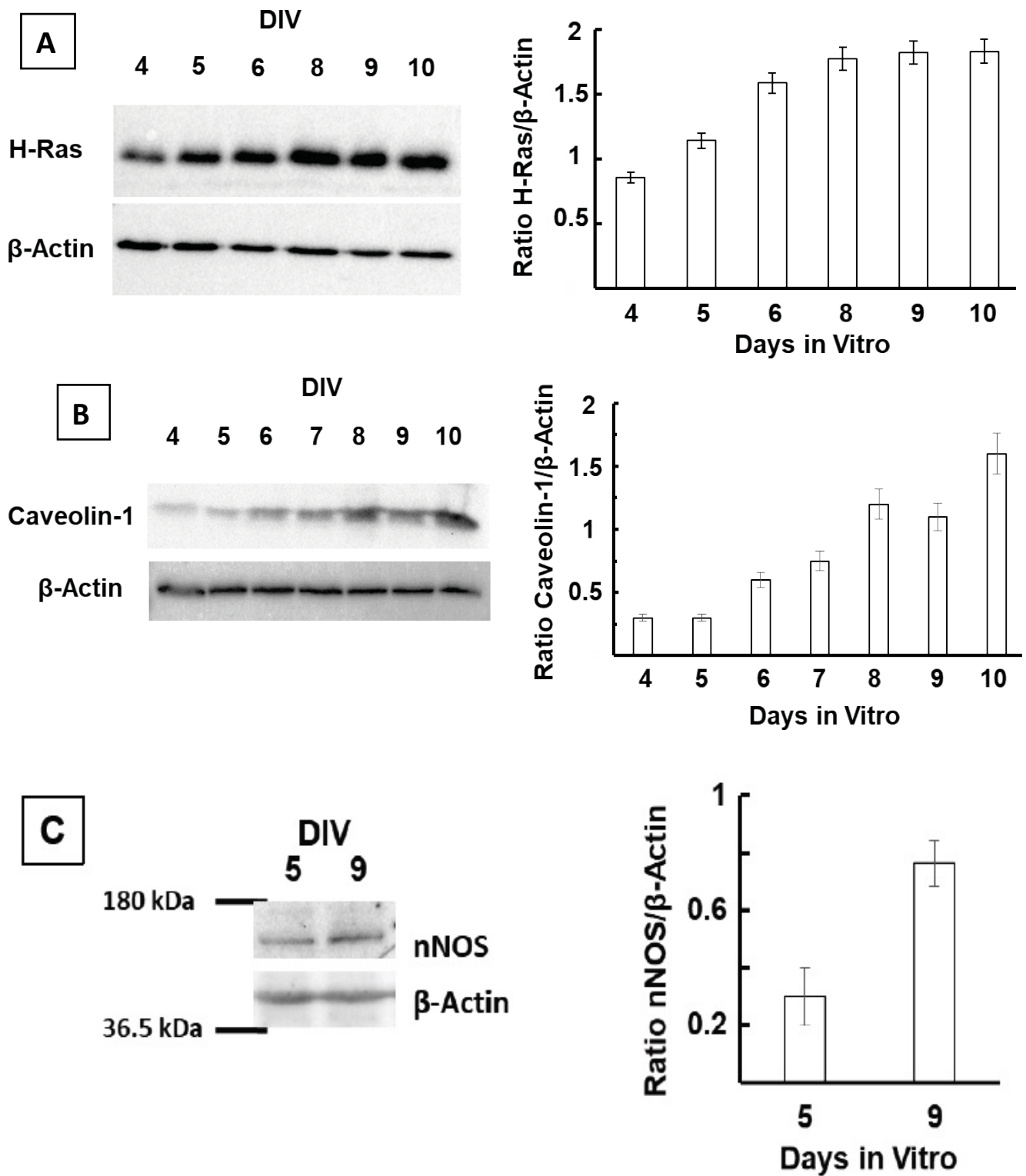
Figure 5. Increase of CGN lipid rafts markers H-Ras and caveolin-1 and of nNOS during CGN maturation *in vitro*. Western blotting of H-Ras (**Panel A**) and caveolin-1 (**Panel B**) in CGN lysates as a function of days in vitro (DIV). **Panel C:** Western blotting of nNOS in CGN lysates at 5 and 9 DIV. The images shown in Panels A, B and C are representative of the results obtained with three different CGN preparations. The results have been plotted in Panels A, B and C as the averages ± s.e. of the ratio of intensities (H-Ras/β-actin), (caveolin-1/β-actin) and (nNOS/β-actin), respectively, versus days in vitro.
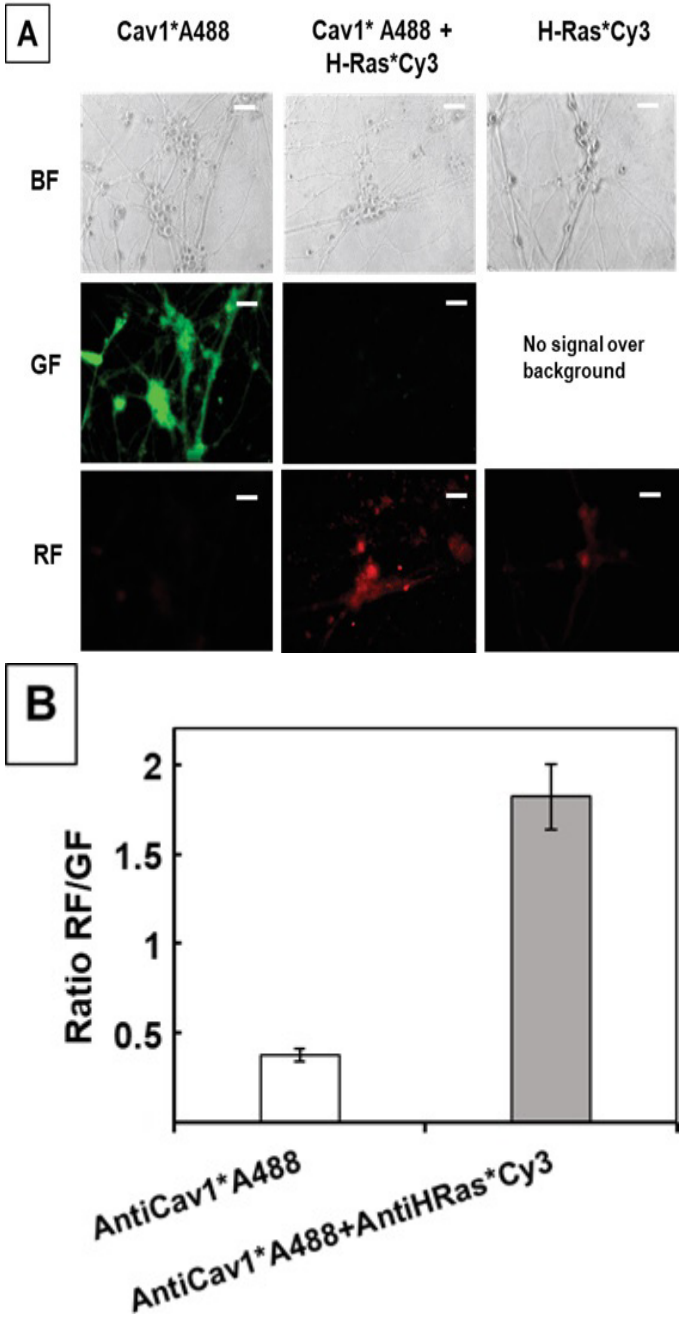
Figure 6. Extensive FRET in CGN from caveolin-1 tagged with IgG-Alexa488 (as FRET donor) to H-Ras tagged with IgG-Cy3 (as FRET acceptor). Panel A: Representative quantitative fluorescence microscopy images of CGN stained with anti-caveolin-1 (sc-894)/IgG-Alexa488 (cav1*A488), with anti-caveolin-1/IgG- Alexa488 and anti-H-Ras (sc-32026)/IgG-Cy3 (cav1*A488/H-Ras*Cy3) and only with anti-H-Ras/IgG-Cy3 (H-Ras*Cy3). Bright-field (BF), green fluorescence (GF) and red fluorescence (RF) images are shown for each one of the selected fields. Green and red frames display the donor and acceptor fluorescence, respectively. Scale bar inserted in fluorescence microscopy images = 10 μm. **Panel B:** Ratio of Red/Green fluorescence intensity per pixel (RF/GF) obtained from the analysis of fluorescence intensity data of CGN somas stained with anti-caveolin-1/IgG-Alexa488 only (cav1*A488) and double stained with anti-caveolin-1/IgG-Alexa488//anti-H-Ras/IgG-Cy3 (cav1*A488/H-Ras*Cy3). The results shown in this panel B are the mean ± s.e. (*) p<0.05, i.e. statistically significant with respect to the control (CGN labeled with the Alexa488 FRET donor only).
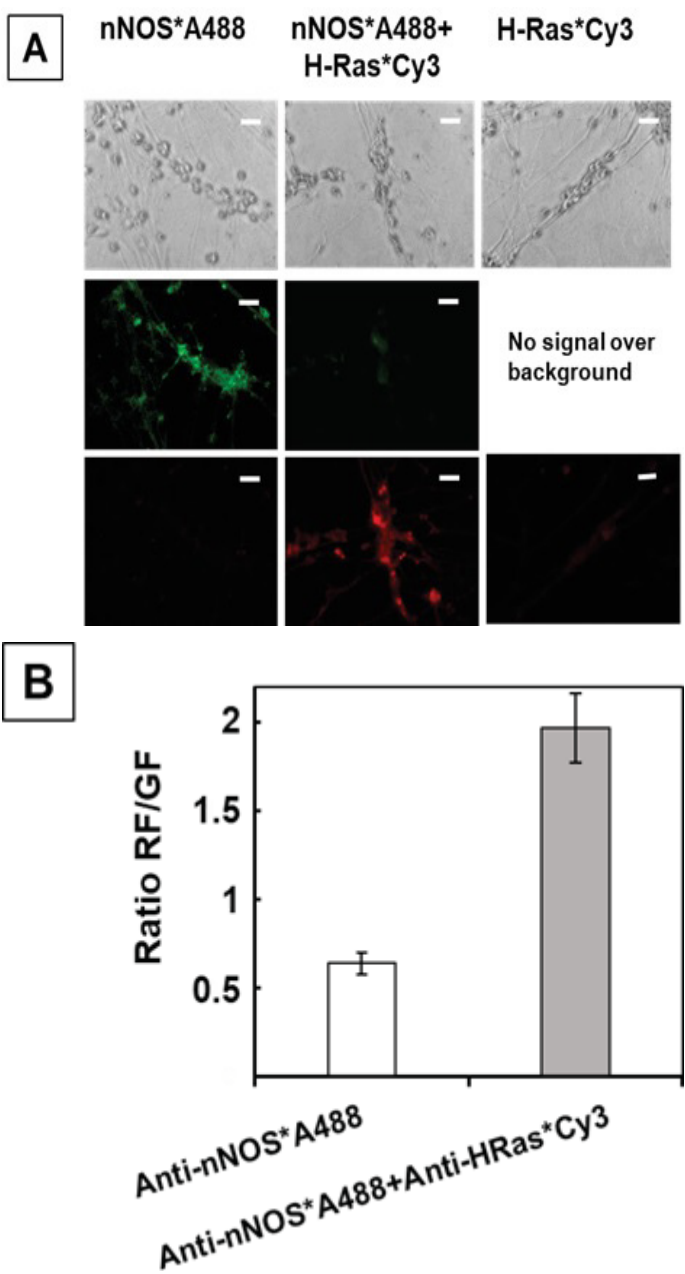
Figure 7. Extensive FRET in CGN from nNOS tagged with IgG-Alexa488 (as FRET donor) to H-Ras tagged with IgG-Cy3 (as FRET acceptor). Panel A: Representative quantitative fluorescence microscopy images of CGN stained with anti-nNOS (sc-5302)/IgG-Alexa488 (nNOS*A488), with anti-nNOS/IgG-Alexa488 and anti-H-Ras (sc-32026)/IgG-Cy3 (nNOS*A488/H-Ras*Cy3) and only with anti-H- Ras/IgG-Cy3 (H-Ras*Cy3). Bright-field (BF), green fluorescence (GF) and red fluorescence (RF) images are shown for each one of the selected fields. Green and red frames display the donor and acceptor fluorescence, respectively. Scale bar inserted in fluorescence microscopy images = 10 μm. **Panel B:** Ratio of Red/Green fluorescence intensity per pixel (RF/GF) obtained from the analysis of fluorescence intensity data of CGN somas stained with anti-nNOS/IgG-Alexa488 only (nNOS*A488) and double-stained with anti-nNOS/IgG-Alexa488//anti-H-Ras/IgG-Cy3 (nNOS*A488/H-Ras*Cy3). The results shown in this panel B are the mean ± s.e. (*) p<0.05, i.e. statistically significant with respect to the control (CGN labeled with the Alexa488 FRET donor only).

The production of ROS that is inhibited by MβCD decreased during CGN maturation and this is reverted by Cb5R3silencing

The production of ROS monitored by H_2DCF-DA decreased between 3 and 4-fold from immature CGN at 5 DIV to mature CGN at 9-10 DIV, and this decrease largely accounts for the ROS production in CGN that is sensitive to MβCD (**Figure 8A**). This result suggested that immature CGN should be more vulnerable to extracellular oxidative neurotoxic insults than mature CGN. We have experimentally assessed this point using 3-morpholinosydnonimine (SIN-1), a superoxide anion and nitric oxide donor that can trigger oxidative CGN death under controlled exposure conditions [43]. Loss of cell viability induced by CGN exposure to 0.5 mM SIN-1 in MLocke's K25 is reduced from 78±2% at 5 DIV to 49±2% at 9-10 DIV.

We have studied the effect of Cb5R3 silencing on ROS production by mature CGN following the protocol indicated in the Materials and Methods, Western blotting showed that we have achieved approximately 50% Cb5R3 silencing at the protein expression level with respect to control CGN, with a statistically non-significant 10-15% decrease of Cb5R3 induced by treatment with control-siRNA (Figure 8B). This partial Cb5R3 silencing produced between 3.5 and 4.5-fold increase of ROS production relative to control and control-siRNA CGN, respectively, when monitored by H_2DCF-DA (Figure 8C).
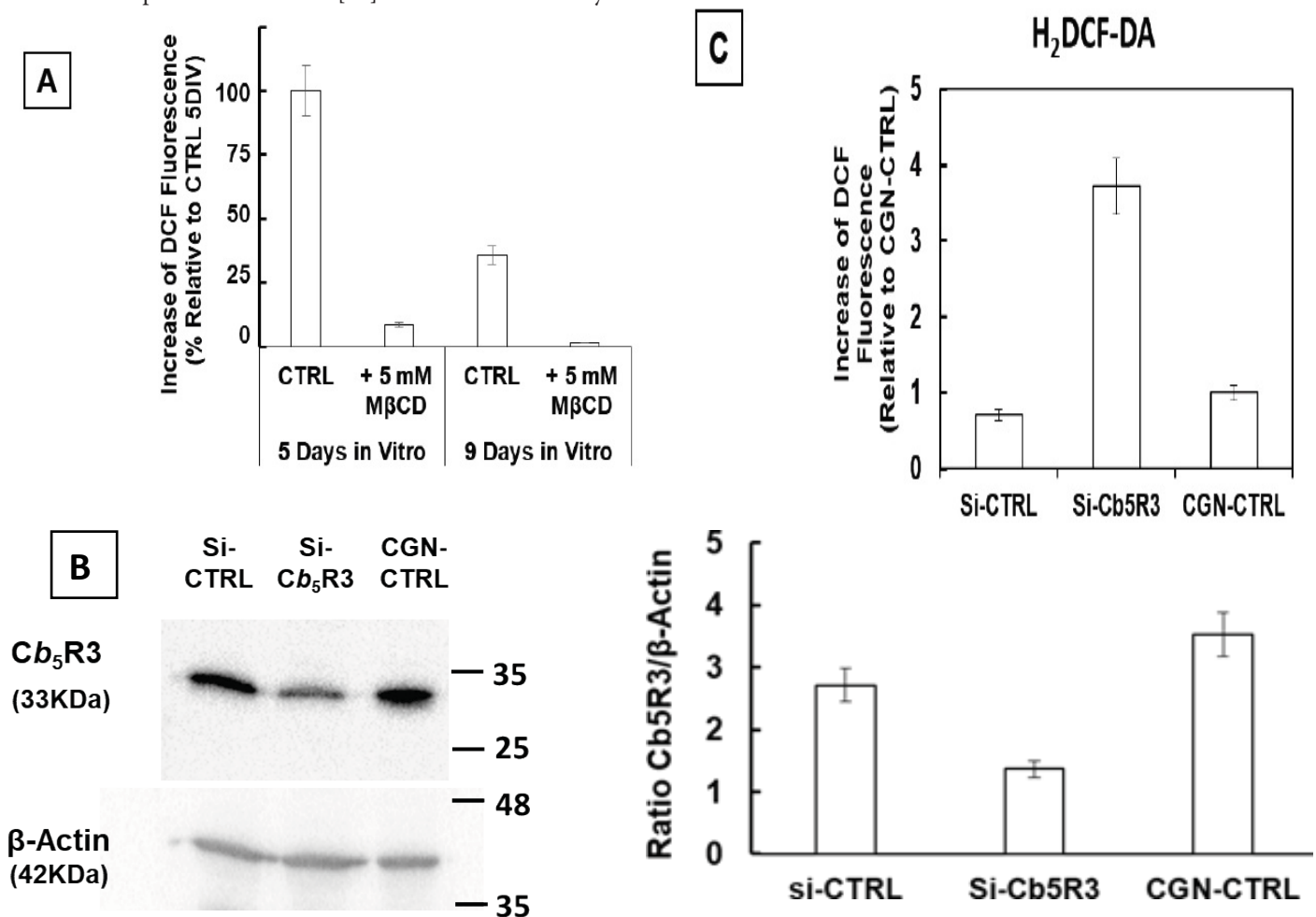

Figure 8. CGN maturation *in vitro* elicits an attenuation of the production of ROS detected by H_2DCF-DA that is impaired by Cb_5R3 silencing. Panel A: CGN production of ROS detected by H_2DCF-DA decay more than 50% from 5 to 9 DIV, and either at 5 and 9 DIV is more than 90% inhibited by 5 min preincubation with 5 mM MβCD. **Panel B:** Treatment of CGN at 4 DIV with si- Cb5R3 RNA during 90 hours (si-Cb5R3) resulted in ~50% and ~60% decrease of Cb5R3 expression with respect to CGN treated with si-Control RNA (si-CTRL) or with respect to untreated CGN (CGN-CTRL), respectively. The images shown in this panel are representative of the results obtained with three different CGN preparations. The results have been plotted as the averages ± s.e. of the ratio of intensities (Cb5R3/β-actin). **Panel C:** CGN production of ROS detected by H_2DCF-DA increases between 3.5 and 4-fold in CGN treated with si-Cb5R3 RNA (si-Cb5R3) with respect to untreated CGN (CGN-CTRL) and with respect to CGN treated with si-Control RNA (si-CTRL). (*) p<0.05, i.e. statistically significant with respect to CGN-CTRL or si-CTRL. The difference between si-CTRL and CGN-CTRL is not statistically significant. The results shown in panels A, B and C are the means± s.e. of experiments performed by triplicate.

DAF2-DA monitors the rapid propagation between neighbor cells and along dendritic extensions of ROS waves induced by irradiation of CGN cultures with light of 470nm

Only 10-15 minutes incubation of CGN with DAF2-DA are needed to acquire bright green fluorescence images, see Figure 9A. The video recording attached as supplementary material of this manuscript (*Supplementary Figure S2*) show that acquisition of images every 5 s with exposure times of 0.05 s to the 470 nm xenon lamp blue-light of the epifluorescence microscope, starting approximately 10-15 s after addition of DAF2-DA to mature CGN, elicited a strong and flash-like increase of the fluorescence intensity at the neurons located close to the center of the light beam.

The sequential images of the video recording (*Supplementary Figure S2*) also show that the flash-like increase of fluorescence rapidly propagates to neighbor cells through neuronal contact sites and dendritic extensions, mimicking a green light-wiring pattern through the longest dendritic extensions. This raised the possibility of a role of the neuronal plasma membrane as a major source of the ROS producing the flash-like increase of fluorescence intensity of DAF2 upon xenon lamp blue light irradiation. This hypothesis was also supported by the large attenuation of the peak intensity of the fluorescence of CGN plus DAF2-DA produced by submillimolar concentrations of MβCD (Figure 9B). Indeed, the concentration of MβCD that elicited 50% of the maximum attenuation of the increase of DAF2 fluorescence intensity in CGN somas was the same that yielded 50% attenuation of the increase of 2',7'-dichlorofluorescein(DCF) fluorescence in CGN somas, compare Figures 9B and 2B.
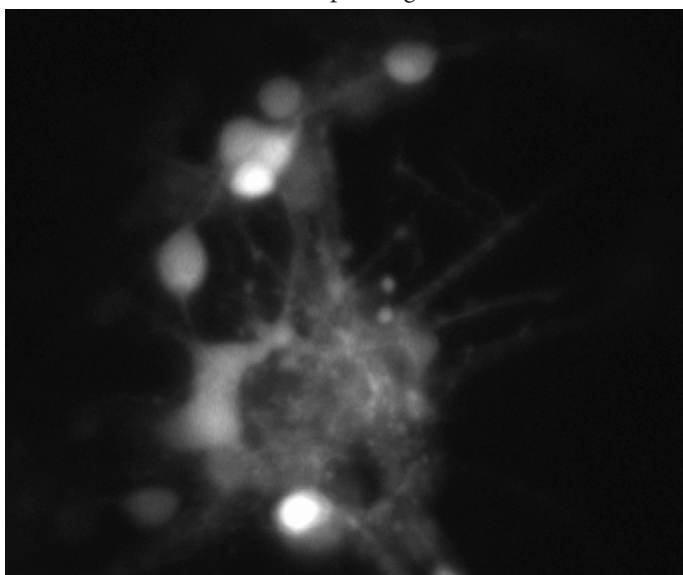
The analysis of the increase of fluorescence intensity in the neuronal soma showed that the fluorescence intensity initially increases slowly and steadily during several minutes and then sharply increases, reaching a peak fluorescence intensity followed by a rapid decay phase only few minutes later (control traces of Figure 9C). For a constant exposure time, the increase of the time interval of images acquisition between light pulses flash-like delays the time at which the flash-like increase of fluorescence intensity is observed and also its amplitude. This a phenomenon caused by ROS produced largely in the vicinity of the neuronal plasma membrane because it is completely blocked by the addition of SOD plus catalase to the extracellular medium. Furthermore, the flash-like increase of fluorescence intensity was also more than 90% attenuated by DPI (Figure 9C). Noteworthy, the concentration of 10 μM DPI produced an almost identical decrease of the amplitude of the flash-like increase of fluorescence intensity of CGN plus DAF2-DA and of the increase of the fluorescence intensity of CGN plus H_2DCF-DA, 80±5% (Figure 9D) and 90±5% (Figure 3C), respectively. Therefore, this result strongly suggested flavoproteins as a common source for the ROS involved in the flash-like increase of fluorescence increase of DAF2-DA and those detected by H_2DCF-DA. However, the steep rise of DFA2 fluorescence is clearly delayed with respect to that of H_2DCF-DA, compare the kinetic traces of Figures 9C and 1D. Since it has been shown that DAF2 fluorescence is enhanced by reactive nitrogen species (RNS) [53,54], this result suggested that DAF2 fluorescence is largely enhanced by ROS/RNS species produced after the ROS species detected by H_2DCF-DA. As peroxynitrite is a major ROS/RNS produced after the reaction between primarily produced ROS (superoxide anion, H_2O_2,..) and RNS (nitric oxide), we studied the effect of the peroxynitrite scavenger MnTBAP to experimentally assess the possibility that peroxynitrite reaction with DAF2 can afford a major contribution to the increase of DAF2 fluorescence observed in our CGN cultures. Indeed, the results showed that 20-50 μM MnTBAP inhibited 60±3% of the flash-like increase of DAF2 fluorescence intensity in CGN (Figure 9E), while 20 μM MnTBAP did not attenuate the increase of fluorescence monitored by H_2DCF-DA (*data not shown*).
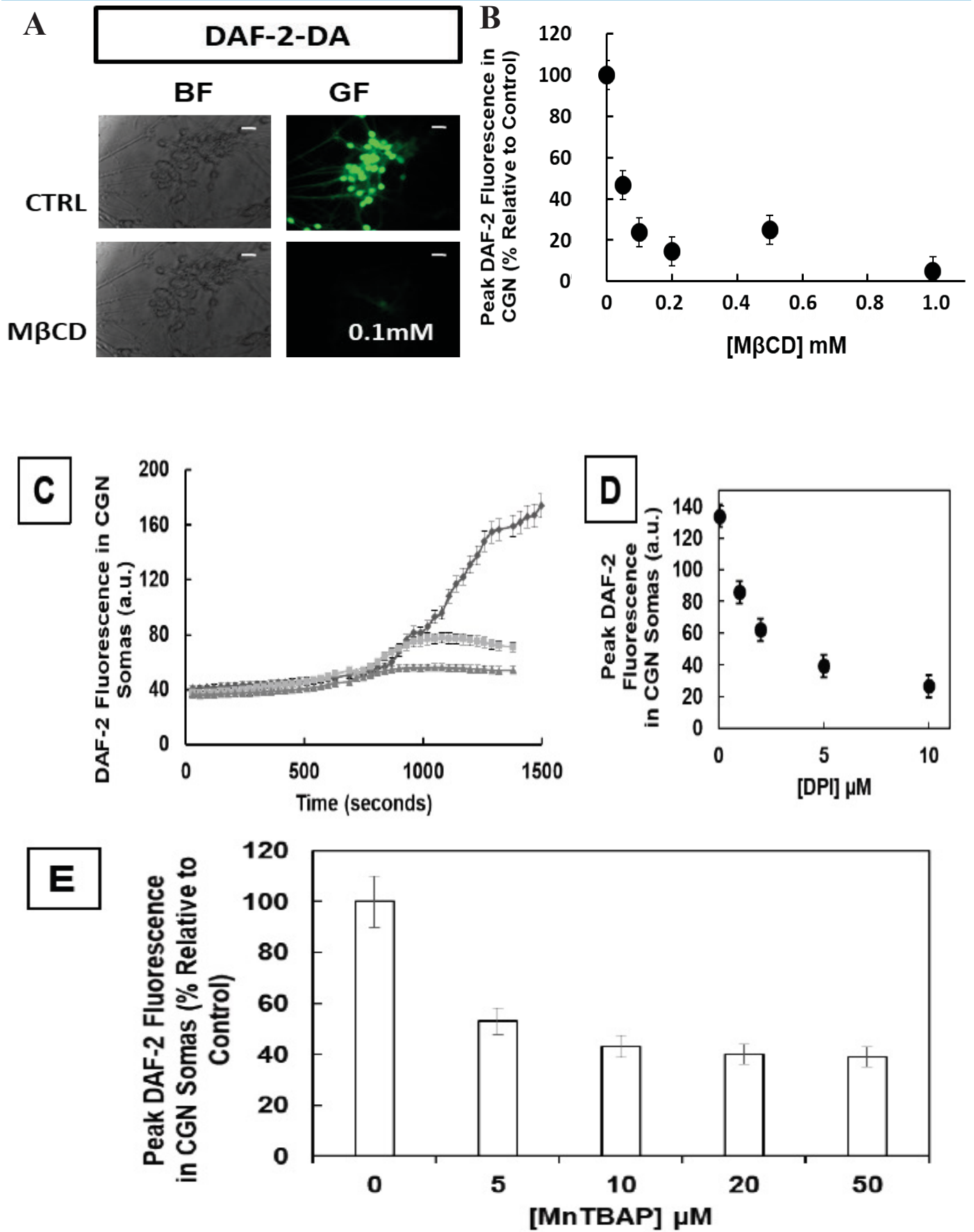
Figure 9. The production of ROS/RNS detected by DAF2-DA in mature CGN is largely inhibited by MβCD, DPI and MnTBAP. Panel A: Representative fluorescence microscopy images of CGN (8-9 DIV) showing that treatment of CGN with MβCD during 5 min almost completely blocks the increase of fluorescence associated with the production of ROS/RNS detected by DAF2-DA at 1200 s after addition of 5 μM DAF2-DA. Bright-field (BF) and green fluorescence (GF) images are shown for each one of the selected fields. Scale bar inserted in fluorescence microscopy images = 10 μm. **Panel B:** Dependence of the maximum increase of the DAF2 fluorescence intensity per pixel in CGN somas (peak DAF2 fluorescence) upon treatment of CGN during 5 min with the indicated MβCD concentrations. Y-axis values have been expressed as percent relative to control (0 MβCD). **Panel C:** Kinetics of the increase of the average DAF2 fluorescence intensity per pixel in CGN somas of CGN at 8-9 DIV in the absence (control, filled circles) and in the presence of 5 μM (filled squares) and 10 μM DPI (filled triangles). **Panel D:** Dependence upon DPI concentration of the peak DAF2 fluorescence intensity per pixel in CGN somas. **Panel E:** Dependence of the peak DAF2 fluorescence intensity per pixel in CGN somas upon treatment of CGN during 5 min with the indicated MnTBAP concentrations. Y-axis values have been expressed as percent relative to control (0 MnTBAP). The results shown in panels B, C, D and E are the means± s.e. of experiments performed by triplicate.

Discussion

The results of this work show that a short-time treatment of CGN with the cholesterol-trapping agent MβCD strongly inhibits the rate of production of ROS by mature CGN in culture. The total duration of the exposure of CGN to MβCD in our experiments has been 15-20 min because fluorescence microscopy images were acquired for 5-10 min after 5 min pre-incubation of CGN with MβCD before placing the Petri dishes in the fluorescence microscope and handlings to focus the selected field for images. As we have shown in a previous and recent publication [38], this treatment with MβCD efficiently extracts cholesterol without producing a significant loss of cell viability in our CGN cultures up to concentrations of MβCD ≥ 20 mM. Here, we show that three different ROS-sensitive dyes, i.e. H_2DCF-DA, DHE and DAF2-DA, monitors a similar and large decrease of ROS production by upon treatment of CGN with MβCD. The large attenuation of the red fluorescence of DHE in CGN by the superoxide anion scavenger Tiron [50,51] excluded the possibility of a significant contribution to the measured red fluorescence of DNA- and RNA-oxidized ethidium complexes formation. As shown with H_2DCF-DA this decrease is significantly attenuated by CGN treatment with MβCD-cholesterol complexes, which prevent cholesterol depletion. Moreover, MβCD-induced decrease of ROS production is widespread in the CGN in culture and well seen both in neuronal somas and extensions. Although DHE is a fluorescence probe that monitors mainly superoxide

anion [45,46], H_2DCF-DA is a ROS probe that monitors a broad range of ROS [45] and DAF2-DA monitors not only nitric oxide but also the production of other ROS, like those generated upon the rapid reaction of nitric oxide with superoxide anion and ascorbate free radicals [48]. Noteworthy, the inhibition of ROS/RNS production monitored by H_2DCF-DA and DAF2-DA is more sensitive to lower concentrations of MβCD than the inhibition of superoxide anion production monitored by DHE. H_2DCF-DA and DHE have been used to show the oxidative stress of CGN during the early stages of apoptosis [14-16,42], in L-glutamate-induced excitotoxic death [3,55,56] and in other oxidative stress-mediated neuronal death [45]. Furthermore, both dyes have been widely used to monitor oxidative-induced cell death in other neuronal cultures. On these grounds, we can conclude that this treatment elicits a generalized and strong impairment of the production of the most relevant ROS involved in oxidative stress-inducing conditions that are neurotoxic for these neurons in culture.

Cholesterol extraction by MβCD has been shown to induce lipid rafts disruption in different cell cultures [36-38]. Therefore, these results suggested a major contribution of lipid rafts to overall ROS/RNS production in our mature CGN cultures. The rapid and nearly complete inhibition of the ROS production monitored by DHE and H_2DCF-DA by extracellularly added SOD strongly support this hypothesis, because SOD does not permeate across the plasma membrane. Furthermore, this result indicates a major role of superoxide anion in the generation of another ROS produced in CGN and detected by H_2DCF-DA. Indeed, the lag phase in the production of ROS detected by H_2DCF-DA, in contrast with the absence of lag phase in the production of superoxide anion monitored with DHE, also gives additional experimental support to this conclusion. A major role of extramitochondrial production of superoxide anion and of ROS detected by H_2DCF-DA is supported also by the fact that the mitochondrial uncoupling protonophores FCCP and DNP produced less than 50% inhibition of the production of these ROS in mature CGN.

Previous works have shown that deregulation of several redox systems associated with neuronal lipid rafts can produce over shots of ROS and/or RNS, namely, superoxide anion by C*b*5R3 [57,58], nitric oxide by nNOS [30,31,59,60], and hydrogen peroxide and superoxide anion by cytochromes P450 [61]. All these redox systems are flavoproteins, and DPI, a broad spectrum flavoprotein inhibitor, produced more than 90% inhibition of ROS/RNS production monitored by the dyes used in this work. In previous works, we have shown that both C*b*5R3

and nNOS are present in caveolin-1/cholesterol-rich lipid rafts of mature CGN [16,30,31,49]. However, the expression of many cytochromes P450 is strongly downregulated in primary neuronal cultures matured in vitro [62], as well as in other growth-stimulated mammalian cell cultures [63]. To experimentally assess this point in our CGN culture we selected the CYP46 isoform of cytochrome P450, which has 24S-cholesterol hydroxylase activity and is a cytochrome P450 isoform that should be expected to be associated with neuronal lipid rafts owing to its important role in brain cholesterol homeostasis [64]. As shown by Western blotting, during CGN maturation in the culture there is strong downregulation of the expression of CYP46 (*Supplementary Figure S3*), and as a result, its expression level in mature CGN is negligible. Noteworthy, we have shown in previous works that there are large differences between the MβCD concentrations needed to inhibit two major calcium systems involved in the control of cytosolic calcium homeostasis of CGN, e.g. LTCCs and N-methyl D-aspartate receptors [31,38]. Therefore, the differences between the potency of inhibition by MβCD of the ROS/RNS production monitored by the different dyes used in this work are likely to be due to the different sensitivity of the redox systems mentioned above and of their regulatory proteins to the extent of lipid rafts disruption by different concentrations of MβCD.
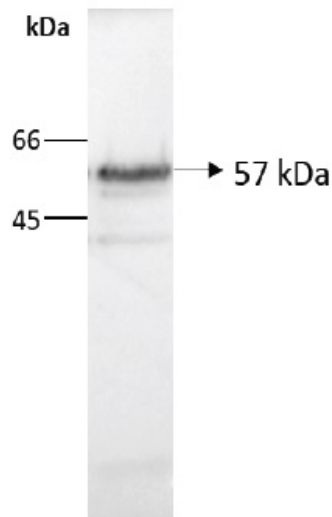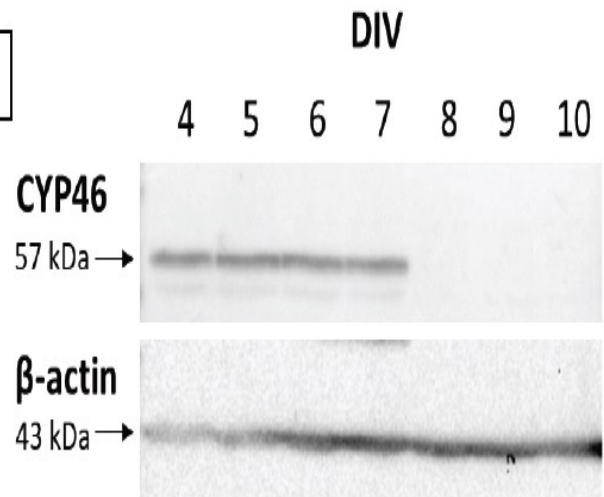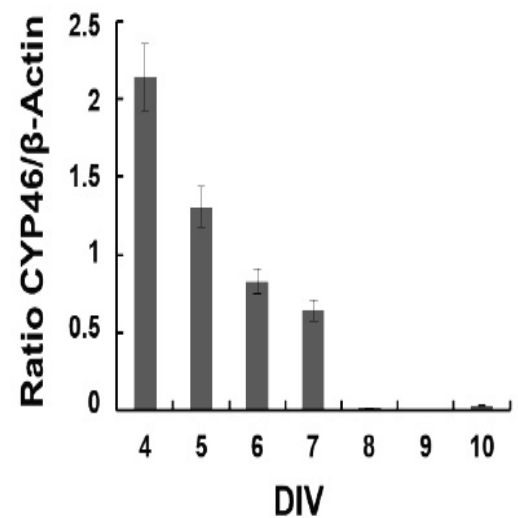

Supplementary Figure S3. Downregulation of CYP46 expression during CGN maturation *in vitro*. Panel A: Western blotting showing the specific immunodetection of CYP46 in CGN lysates (4 DIV) with goat anti-CYP46 (Santa Cruz Biotechnology sc-74391, 1:100 dilution). **Panel B:** Immunodetection of CYP46 in CGN lysates as a function of days *in vitro* (DIV). After immunodetection of CYP46 with goat anti-CYP46 (Santa Cruz Biotechnology sc-74 391, 1:100 dilution), the PVDF membrane was washed and stripped as indicated in the Materials and Methods and used for immunodetection of β-actin with monoclonal mouse anti-β-actin (Sigma- Aldrich A1978, 1:200 dilution). The images shown are representative of the results obtained with three different CGN preparations. The results have been plotted in **Panel C** as the means ±s.e. of the ratio of intensities (CYP46/β-actin) versus days *in vitro*.

Fluorescence microscopy images of CGN stained with fluorescent cholera toxin B and Western blotting of H-Ras content show more than two-fold increase of lipid rafts per neuron during the maturation of CGN cultures *in vitro*. Noteworthy, these increases are similar to the increase during maturation of CGN of redox systems associated with these lipid rafts, namely, ~2.5-fold increase of Cb5R3[16,22] and ~2.5-fold increase of nNOS (this work). This latter result is in good agreement with the results reported by others during cerebellum maturation [65,66]. Moreover, FRET imaging results show that nNOS and the protein lipid rafts marker H-Ras are within the FRET distance range for the experimental approach used in this work. As discussed in previous works of our group [30,31,49],using this experimental FRET approach with fluorescent antibodies this means that they are at a distance ≤80 nm. Therefore, we can conclude that both nNOS and H-Ras are within the same lipid rafts. In previous works, we reached the same conclusion for Cb5R3[31,49].

On the other hand, mature CGN at 9-10DIV are more resistant than immature CGN at 5DIV to the oxidative insult produced by extracellular exposure to SIN-1, a ROS/RNS releasing compound [67,68] that has been shown to mimic the extracellular oxidative stress associated with inflammation and ischemia-reperfusion in mammalian brain [32,68,69]. Consistently, we found that CGN maturation leads to a large decrease of the production of ROS detected by H$_2$DCF-DA. This attenuation of ROS production in mature CGN can be reverted by silencing the expression of Cb5R3 to approximately 50%. Cb5R3 is a redox protein associated with lipid rafts, whose expression level increases approximately 2.5-fold from 5DIV to 9-10DIV [22], and whose deregulation leads to an overshot of superoxide anion production by CGN [16] and also of rat brain synaptic plasma membranes [14,57]. Therefore, our results show that Cb5R3 plays a major role in the attenuation of the overall ROS production in mature CGN, and reveal a major role of this protein as an antioxidant cellular defense against CGN exposure to extracellular neurotoxic oxidative insults.

DAF2 is a fluorescent dye that, besides being useful for nitric oxide detection under controlled experimental conditions [53,54], it has been shown to be largely photoactivated upon the irradiation with the 490nm light of a fluorescence microscope xenon lamp [54]. A remarkable photoactivation pattern is displayed by CGN stained with DAF2- DA upon irradiation with the fluorescence microscope Xenon lamp 470 nm blue light. The kinetics of ROS production by CGN detected with DAF2-DA is more than 90% inhibited by CGN pre-treatment with MβCD or DPI, as also found for the ROS production monitored with H$_2$D-

CF-DA. However, DAF2-DA revealed the occurrence of a clear space-temporal pattern of the increase of fluorescence within the CGN culture. Sequential images showed that a flash-like peak of fluorescence initiates at the center of the field irradiated with the light beam and rapidly spread away across neighbor neurons and through the dendritic extensions. This is a spreading fluorescent wave induced by ROS/RNS because it is approximately 70% attenuated by the peroxynitrite scavenger MnTBAP, and it is completely blocked by addition of SOD plus catalase to the extracellular medium. In addition, the latter result points out that it is largely due to ROS produced at or near the neuronal plasma membrane. Thus, ROS propagation in the culture is not isotropic, and the images sequences strongly suggest that ROS propagates along the neuronal plasma membrane. Taking into account that images were acquired every 5 s and the fluorescence propagation distance observed between sequential images in dendritic extensions, we can calculate a ROS propagation rate higher than 10 μm/s. The possibility that this was reflecting a depolarizing wave can be excluded because it is not affected by preincubation of the CGN with 1 μM tetrodotoxin (*Supplementary Figure S4*). DAF2 complexation with calcium may also enhance the fluorescence of this dye [54]. However, the flash-like peak of DAF2-DA fluorescence was not affected by preincubation of CGN with 10 μM nifedipine nor by 10 μM MK-801, i.e. by inhibitors of LTCCs and N-methyl D-aspartate receptors which are the two major calcium entry systems present in the plasma membrane of these neurons (*Supplementary Figure S4*). Therefore, these results reveal for the first time to the best of our knowledge rapid ROS wiring phenomena along with the dendritic extensions of mature CGN in culture.
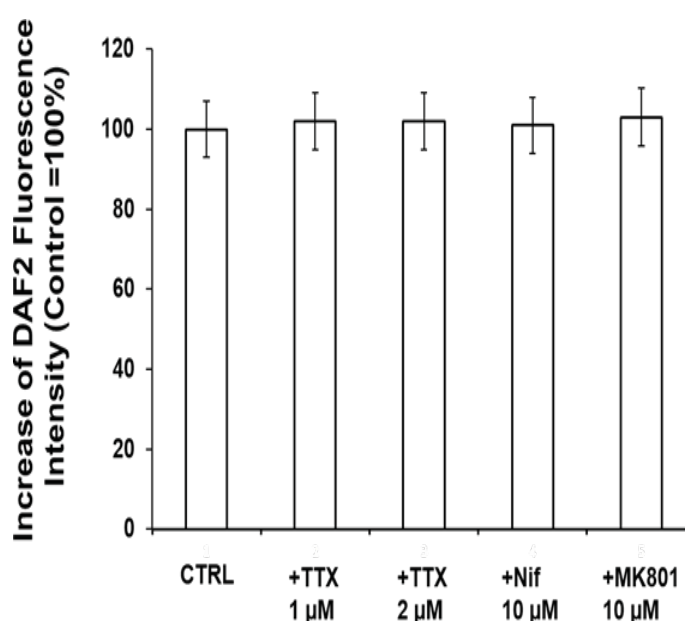
In summary, the results of this work unravel a major role of lipid rafts of the plasma membrane to the control of the overall ROS production by CGN in culture under partially depolarizing conditions that promote neuronal survival, with a major contribution of the lipid raft-associated Cb5R3 in this biological function. Moreover, lipid rafts of the plasma membrane also provide key structural elements to speed up ROS signaling propagation between neurons in mature CGN in culture.

Acknowledgments

References

1] Choi DW (1998) Glutamate neurotoxicity and diseases of the nervous system. Neuron1:623–634.

2] Beal MF (2000) Energetics in the pathogenesis of neurodegenerative diseases. Trends Neurosci.23:298–304.

3] Atlante A, Calissano P, Bobba A, Giannattasio S, Marra E, Passarella S (2001) Glutamate neurotoxicity, oxidative stress and mitochondria. FEBS Lett. 497:1-5.

4] Andrus PK, Fleck TJ, Gurney ME, Hall ED (1998) Protein oxidative damage in a transgenic mouse model of familial amyotrophic lateral sclerosis. J. Neurochem.71: 2041-2048.

5] Cicchetti F, Drouin-Ouellett J, Gross RE (2009) Environmental toxins and Parkinson's disease: what have we learned from pesticide-induced animal models? Trends Pharmacol Sci 30: 475-483.

6] Sugimoto K, Iadecola C (2003) Delayed effect of administration of COX-2inhibitor in mice with acute cerebral ischemia. Brain Res.960: 273-276.

7] Gutierrez-Merino C, López-Sánchez C, Lagoa R, Samhan-Arias AK, Bueno C, García-Martínez V (2011) Neuroprotective actions of flavonoids. CurrentMedicinal Chemistry18: 1195-1212.

8] Iadecola C (1997) Bright and dark sides of nitric oxide in ischemic brain injury. Trends Neurosci.20: 132-139.

9] Beal MF (2002) Oxidatively modified proteins in aging and disease. FreeRadic Biol Med 32: 797-803.

10] Praticò D, Delanty N (2000) Oxidative injury in diseases of the central nervous system: Focus on Alzheimer's disease. Am. J. Med.109: 577-585.

11] Blesa J, Trigo-Damas I, Quiroga-Varela A, Jackson-Lewis VR (2015) Oxidative stress and Parkinson's disease. Front Neuroanat 9:91.doi: 10.3389/fnana.2015.00091. eCollection 2015.

12] Butterfield DA, Halliwell B (2019) Oxidative stress, dysfunctional glucose metabolism, and Alzheimer's disease. Nat Rev Neurosci 20:148-160.

13] Martin-Romero FJ, Garcia-Martin E, Gutierrez-Merino C (1996) Involvement of free radicals in the signaling of low-potassium induced apoptosis in cultured cerebellar granule cells. Int J Dev Biol, Suppl.1,197S-198S.

14] Martin-Romero FJ, Garcia-Martin E, Gutierrez-Merino C (2002) Inhibition of the oxidative stress produced by plasma membrane NADH oxidase delays low- potassium induced apoptosis of cerebellar granule cells. J Neurochem 82: 705–715.

15] Valencia A, Morán J (2001) Role of oxidative stress in the apoptotic cell death of cultured cerebellar granule cells. J Neurosci Res.64: 284–297.

16] Samhan-Arias AK, Marques-da-Silva D, Yanamala N, Gutierrez-Merino C (2012) Stimulation and clustering of cytochrome b5 reductase in caveolin-rich lipid microdomains is an early event in oxidative stress-mediated apoptosis of cerebellar granule neurons. J Proteomics 75: 2934-2949.

17] Mao GD, Poznansky MJ (1992) Electron spin resonance study on the permeability of superoxide radicals in lipid bilayers and biological membranes. FEBS Lett.305: 233–236.

18] Herrero A, Barja G (2000) Localization of the site of oxygen radical generation inside the complex I of heart and non-synaptic brain mammalian mitochondria. J. Bioenerg. Biomembr.32: 609-615.

19] Bedard K, Krause KH (2007) The NOX family of ROS-generating NADPH oxidases: physiology and pathophysiology. Physiol. Rev.87: 245-313.

20] Martin-Romero FJ, Gutierrez-Martin Y, Henao F, Gutierrez-Merino C (2002) The NADH oxidase activity of the plasma membrane of synaptosomes is a major source of superoxide anion and is inhibited by peroxynitrite. J Neurochem 82: 604–614.

21] Samhan-Arias AK, Duarte RO, Martin-Romero FJ, Moura JJG, Gutierrez-Merino C (2008) Reduction of ascorbate free radical by the plasma membrane of synaptic terminals from rat brain. Arch. Biochem. Biophys. 469: 243–254.

22] Samhan-Arias AK, Garcia-Bereguiain MA, Martin-Romero FJ, Gutierrez-Merino C (2009) Clustering of plasma membrane-bound cytochrome b5 reductase within 'lipid rafts' microdomains of the neuronal plasma membrane. Mol Cell Neurosci 40: 14–26.

23] Samhan-Arias AK, López-Sánchez C, Marques-da-Silva D, Lagoa R, et al. (2016) High expression of cytochrome b5 reductase isoform 3/cytochrome b5 system in the cerebellum and pyramidal neurons of adult rat brain. Brain Struct. Funct. 221: 2147-2162.

24] Percy MJ, Lappin TR (2008) Recessive congenital methemoglobinemia: cytochrome b5 reductase deficiency. British Journal of Haematology141: 298-308.

25] Ewenczyk C, Leroux A, Roubergue A, Laugel V, Afenjar A, et al. (2008) Recessive hereditary methemoglobinemia, type II: delineation of the clinical spectrum. Brain 131: 760- 761.

26] Leroux A, Junien C, Kaplan J, Bambenger J (1975) Generalised deficiency of cytochrome b5 reductase in congenital methemoglobinemia with mental retardation. Nature 258: 619-620.

27] Toelle SP, Boltshauser E, Mössner E, Zurbriggen K, Eber S (2004) Severe neurological impairment in hereditary methemoglobinemia type 2. Eur. J.Pediatr. 163: 207–209.

28] Aalfs CM, Salieb-Beugelaar GB, Wanders RJA, Mannens MMAM, Wijburg FA (2000) A case of methemoglobinemia type II due to NADH-cytochrome b5reductase deficiency: determination of the molecular basis. Hum. Mutat.16:18-22.

29] Sato Y, Sagami I, Shimizu T (2004) Identification of Caveolin-1-interacting sites in Neuronal Nitric-oxide Synthase. J. Biol. Chem.279: 8827-8836.

30] Marques-da-Silva D, Gutierrez-Merino C (2012) L-type voltage-operated calcium channels, N-methyl-D- aspartate receptors and neuronal nitric-oxide synthase form a calcium/redox nano-transducer within lipid rafts. Biochem. Biophys. Res. Commun. 420:257-262.

31] Marques-da-Silva D, Gutierrez-Merino C (2014) Caveolin-rich lipid rafts of the plasma membrane of mature cerebellar granule neurons are microcompartments for calcium/reactive oxygen and nitrogen species cross-talk signaling. Cell Calcium 56: 108-123.

32] Szabo C, Ischiropoulos H, Radi R (2007) Peroxynitrite: biochemistry, pathophysiology, and development of therapeutics. Nat. Rev. Drug Discov.6: 662-680.

33] Bolaños JP, Almeida A, Stewart V, Peuchen S, et al. (1997) Nitric oxide-mediated mitochondrial damage in the brain: mechanisms and implications for neurodegenerative diseases. J. Neurochem.68: 2227-2240.

34] van der Veen RC, Hinton DR, Incardonna F, Hofman FM (1997) Extensive peroxynitrite activity during progressive stages of central nervous system inflammation. J. Neuroimmunol.77:1-7.

35] Liu D, Ling X, Wen J, Liu J (2000) The role of reactive nitrogen species in secondary spinal cord injury: formation of nitric oxide, peroxynitrite, and nitrated protein. J. Neurochem.75: 2144-2154.

36] Barman S, Nayak DP (2007) Lipid Raft Disruption by Cholesterol Depletion Enhances Influenza A Virus Budding from MDCK Cells. J. Virol.81:12169-12178.

37] Lu J-C, Chiang Y-T, Lin Y-C, Chang Y-T, Lu C-Y, et al. (2016) Disruption of Lipid Raft Function Increases Expression and Secretion of Monocyte Chemoattractant Protein-1 in 3T3-L1 Adipocytes. PLOS One 11: e0169005.

38] Fortalezas S, Marques-da-Silva D, Gutierrez-Merino C (2018) Methyl- β- cyclodextrin impairs the phosphorylation of the β2-subunit of L-type of calcium channels and cytosolic calcium homeostasis in mature cerebellar granule neurons. International Journal of Molecular Sciences 19: 3667-3688.

39] López-Nicolás JM, Rodríguez-Bonilla P, García-Carmona F (2014) Cyclodextrins and Antioxidants. Critical Reviews in Food Science and Nutrition 54: 251-276.

40] Tiwari G, Tiwari R, Rai AK (2010) Cyclodextrins in delivery systems: Applications. J. Pharm. Bioallied Sci. 2: 72-79.

41] Shelley RH, Babu J (2018) Role of Cyclodextrins in Nanoparticle-Based Drug Delivery Systems. Journal of Pharmaceutical Sciences107:1741-1753.

42] Samhan-Arias AK, Martín-Romero FJ, Gutierrez-Merino C (2004) Kaempferol blocks oxidative stress in cerebellar granule cells and reveals a key role for the plasma membrane NADH oxidase activity in the commitment of apoptosis. Free Radical Biology and Medicine 37: 48-61.

43] Gutierrez-Martín Y, Martin-Romero FJ, Henao F, Gutierrez-Merino C (2005) Alteration of cytosolic free calcium homeostasis SIN-1: High sensitivity of L-type Ca^{2+}-channels to extracellular oxidative/nitrosative stress in cerebellar granule neurons. J. Neurochem. 92: 973-989.

44] Fortalezas S, Marques-da-Silva D, Gutierrez-Merino C (2018) Creatine protects against cytosolic calcium dysregulation, mitochondrial depolarization and increase of reactive oxygen species production in rotenone-induced cell death of cerebellar granule neurons. Neurotoxicity Research 34:717-732.

45] Wardman P (2007) Fluorescent and luminescent probes for measurement of oxidative and nitrosative species in cells and tissues: progress, pitfalls, and prospects. Free Radic. Biol. Med. 43: 995-1022.

46] Zhao H, Kalivendi S, Zhang H, Joseph J, Nithipatikom K, Vasquez-Vivar J, Kalyanaraman B (2003) Superoxide reacts with hydroethidine but forms a fluorescent product that is distinctly different from ethidium: potential implications in intracellular fluorescence detection of superoxide. Free Radic. Biol. Med.34:1359-1368.

47] Zielonka J, Hardy M, Kalyanaraman B (2009) HPLC study of oxidation products of hydroethidine in chemical and biological systems: ramifications in superoxide measurements. Free Radic. Biol. Med.46: 329-338.

48] McQuade LE, Lippard SJ (2010) Fluorescent probes to investigate nitric oxide and other reactive nitrogen species in biology (truncated form: fluorescent probes of reactive nitrogen species). Curr. Opin. Chem. Biol.14: 43-49.

49] Marques-da-Silva D, Samhan-Arias AK, Tiago T, Gutierrez-Merino C (2010) L- type calcium channels and cytochrome b5 reductase are components of protein complexes tightly associated with lipid rafts microdomains of the neuronal plasma membrane. J Proteomics73: 1502-1510.

50] Krishna CM, Liebmann JE, Kaufman D, DeGraff W, Hahn SM, McMurry T, Mitchel JB, Russo A (1992) The catecholic metal sequestering agent 1,2- dihydroxybenzene-3,5-disulfonate confers protection against oxidative cell damage. Arch. Biochem. Biophys. 294: 98-106.

51] Kim JS, Cho EW, Chung HW, Kim IG (2006) Effects of Tiron, 4,5-dihydroxy-1,3- benzene disulfonic acid, on human promyelotic HL-60 leukemia cell differentiation and death. Toxicology 223: 36-45.

52] Toescu EC (1999) Activity of voltage-operated calcium channels in rat cerebellar granule neurons and neuronal survival. Neuroscience 94: 561-570.

53] Kojima H, Nakatsubo N, Kikuchi K, Kawahara S, Kirino Y, Nagoshi H, HirataY, Nagano T (1998) Detection and Imaging of Nitric Oxide with Novel Fluorescent Indicators: Diaminofluoresceins. Anal. Chem.70: 2446-2453.

54] Broillet M-C, Randin O, Chatton J-Y (2001) Photoactivation and calcium sensitivity of the fluorescent NO indicator 4,5-diaminofluorescein (DAF-2): implications for cellular NO imaging. FEBS Letters 491:227-232.

55] Reynolds IJ, Hastings TG (1995) Glutamate induces the production of reactive oxygen species in cultured forebrain neurons following NMDA receptor activation. J. Neurosci.15: 3318-3327.

56] Jacobs CM, Aden P, Mathisen GH, Khuong E, et al. (2006) Chicken cerebellar granule neurons rapidly develop excitotoxicity in culture. J. Neurosci. Methods 156: 129-135.

57] Samhan-Arias AK, Fortalezas S, Cordas CM, Moura I, Moura JJG, Gutierrez- Merino C (2018) Cytochrome b5 reductase is the component from neuronal synaptic plasma membrane vesicles that generates superoxide anion upon stimulation by cytochrome c. Redox Biology15:109-114.

58] Samhan-Arias AK, Gutierrez-Merino C (2014) Purified NADH-Cytochromeb5 Reductase Is a Novel Superoxide Anion Source Inhibited by Apocynin: Sensitivity to nitric oxide and peroxynitrite. Free Radic. Biol. Med.73: 174-189.

59] Zhou L, Zhu D-Y (2009) Neuronal nitric oxide synthase: Structure, subcellular localization, regulation, and clinical implications. Nitric Oxide 20: 223-230.

60] Gutierrez-Merino C, Marques-da-Silva D, Fortalezas S, Samhan-AriasAK (2014) Cytosolic calcium homeostasis in neurons: Control systems, modulation by reactive oxygen and nitrogen species, and space and time fluctuations. In Heinbockel T (Ed), Neurochemistry (ISBN 980-953-307-1129-7), InTech, Rijeka (Croatia), Chapter 3, pp. 59-110.

61] Schenkman JB, Jansson I (2003) The many roles of cytochrome b5.J. Pharmacol. Ther.97:139-152.

62] Mulero-Navarro S, Santiago-Josefat B, Pozo-Guisado E, et al. (2003) Down-regulation of CYP1A2 induction during the maturation of mouse cerebellar granule cells in culture: role of nitric oxide accumulation. Eur. J. Neurosci.18: 2265-2272.

63] Tinel M, Berson A, Elkahwaji J, Cresteil T, Beaune P, Pessayre D (2003) Downregulation of cytochromes P450 in

growth-stimulated rat hepatocytes: role of c- Myc induction and impaired C/EBP binding to DNA. J. Hepatol. 39: 171-178.

64] Moutinho M, Nunes MJ, Rodrigues E (2016) Cholesterol 24-hydroxylase: Brain cholesterol metabolism and beyond. Biochem. Biophys. Acta –Molecular and Cell Biology of Lipids1861: 1911-1920.

65] Schilling K, Schmidt HH, Baader SL (1994) Nitric oxide synthase expression reveals compartments of cerebellar granule cells and suggests a role for mossy fibers in their development. Neuroscience 59: 893-903.

66] Li M, Wang L, Peng Y, Wang JC, Zhou LH (2010) Knockdown of the neuronal nitric oxide synthase gene retard the development of the cerebellar granule neurons in vitro. Dev. Dyn. 239: 474-481.

67] Kelm M, Dahmann R, Wink D, Feelisch M (1997) The nitric oxide/superoxide assay. Insights into the biological chemistry of the NO/O_2^{-} interaction. J. Biol. Chem. 272: 9922-9932.

68] Martín-Romero FJ, Gutiérrez-Martín Y, Henao F, Gutierrez-Merino C (2004) Fluorescence measurements of steady state peroxynitrite production upon SIN-1 decomposition: NADH versus dihydro dichlorofluorescein and dihydrorhodamine123.J. Fluorescence 14:17-23.

69] Bao F, Liu D (2002) Peroxynitrite generated in the rat spinal cord induces neuron death and neurological deficits. Neuroscience115: 839-849.